Atmos. Chem. Phys. Discuss., 9, 8469–8539, 2009
www.atmos-chem-phys-discuss.net/9/8469/2009/

Atmospheric Chemistry and Physics Discussions

This discussion paper is/has been under review for the journal *Atmospheric Chemistry and Physics (ACP)*. Please refer to the corresponding final paper in *ACP* if available.

Observations of heterogeneous reactions between Asian pollution and mineral dust over the Eastern North Pacific during INTEX-B

C. S. McNaughton[1], A. D. Clarke[1], V. Kapustin[1], Y. Shinozuka[1,*], S. G. Howell[1], B. E. Anderson[2], E. Winstead[2], J. Dibb[3], E. Scheuer[3], R. C. Cohen[4], P. Wooldridge[4], A. Perring[4], L. G. Huey[5], S. Kim[5], J. L. Jimenez[6], E. J. Dunlea[6], P. F. DeCarlo[6,], P. O. Wennberg[7], J. D. Crounse[7], A. J. Weinheimer[8], and F. Flocke[8]**

[1]School of Ocean and Earth Science and Technology, University of Hawaii, Honolulu, HI, 96822, USA
[2]NASA Langley Research Center, Hampton, VA, 23665, USA
[3]University of New Hampshire, Durham, NH, 03824, USA
[4]University of California Berkeley, Berkeley, CA, 94720, USA
[5]Georgia Institute of Technology, Atlanta, GA, 30332, USA

[6]Cooperative Institute for Research in Environmental Sciences (CIRES) and University of Colorado, Boulder, CO, 80309, USA
[7]California Institute of Technology, Pasadena, CA, 91125, USA
[8]National Center for Atmospheric Research, Boulder CO, 80307, USA
[*]now at: NASA Ames Research Center, Moffett Field, CA, 94035, USA
[**]now at: Paul Scherrer Institute, Switzerland

Received: 19 February 2009 – Accepted: 20 February 2009 – Published: 31 March 2009

Correspondence to: C. S. McNaughton (csmcnaug@hawaii.edu)

Published by Copernicus Publications on behalf of the European Geosciences Union.

Abstract

In-situ airborne measurements of trace gases, aerosol size distributions, chemistry and optical properties were conducted over Mexico and the Eastern North Pacific during MILAGRO and INTEX-B. Heterogeneous reactions between secondary aerosol precursor gases and mineral dust during long-range transport lead to irreversible sequestration of sulfur and nitrogen compounds in the supermicrometer particulate size range.

Simultaneous measurements of aerosol size distributions and weak-acid soluble calcium result in an estimate of 11 wt% of $CaCO_3$ for Asian dust. During transport across the North Pacific, 10–30% of the $CaCO_3$ is converted to $CaSO_4$ or $Ca(NO_3)_2$ through reactions with trace gases. The 11-year record from the Mauna Loa Observatory confirm these findings, indicating that, on average, 16% of the $CaCO_3$ has reacted to form $CaSO_4$ and 14% has reacted to form $Ca(NO_3)_2$. Heterogeneous reactions resulting in ~3% increase in dust solubility is shown to have an insignificant effect on their optical properties compared to their variability in-situ. However, competition between supermicrometer dust and submicrometer primary aerosol for condensing secondary aerosol species led to a 25% smaller number median diameter for the accumulation mode aerosol. A 10–25% reduction of accumulation mode number median diameter results in a 30–70% reduction in submicrometer light scattering at relative humidities in the 80–95% range. At 80% RH submicrometer light scattering is only reduced ~3% due to a higher mass fraction of hydrophobic refractory components in the dust-affected accumulation mode aerosol. Thus reducing the geometric mean diameter of the submicrometer aerosol has a much larger effect on aerosol optics than changes to the hygroscopic:hydrophobic mass fractions of the aerosol.

In the presence of dust, nitric acid concentrations are reduced to <50% of total nitrate (nitric acid plus particulate nitrate). NO_y as a fraction of total nitrogen (NO_y plus particulate nitrate), is reduced from >85% to 60–80% in the presence of dust. These observations support previous model studies which predict irreversible sequestration of reactive nitrogen species through heterogeneous reactions with mineral dust during

ACPD

9, 8469–8539, 2009

long-range transport.

1 Introduction

Mineral aerosol is generated at the Earth surface by aeolian erosion of unconsolidated sand to clay grade soil particles. Under specific meteorological conditions, large dust storms can loft mineral dust directly into the FT where they can be transported intercontinentally (Clarke et al., 2001; Husar et al., 2001; Prospero, 1999).

Mineral aerosol participate in a wide variety of atmospheric process including direct radiative forcing (Sokolik and Toon, 1999; Tegen and Lacis, 1996), indirectly as cloud and ice condensation nuclei (Charlson et al., 1992; Sassen, 2002; Sassen et al., 2003), as a source of micronutrients in biogeochemical cycles (Harvey, 2007; Martin, 1990), and as surfaces for heterogeneous chemical reactions (Andreae and Crutzen, 1997; Dentener et al., 1996; Song and Carmichael, 2001). Laboratory measurements have shown that metal oxides (e.g. CaO, MgO) as well as carbonates ($CaCO_3$) in African and Asian dust samples can facilitate the oxidation of SO_x (Ullerstam et al., 2002; Usher et al., 2002) and NO_x species (Grassian, 2001; Underwood et al., 2001). Climate models are incorporating these heterogeneous reactions because they irreversibly transfer these species from the gas- to the particulate-phase (Phadnis and Carmichael, 2000; Song and Carmichael, 2001), affecting the concentrations of tropospheric oxidants (Jacob, 2000; Martin et al., 2003; Tang et al., 2004) and global radiative forcing (Bauer and Koch, 2005; Liao and Seinfeld, 2005).

Estimates of present day dust emissions fluxes are on the order of 1000–3000 $Tg\,yr^{-1}$ (Dentener et al., 1996, 2006; Ginoux et al., 2001). The total all-models-average for the global climate models (GCMs) participating in the AeroCom project is 1840 $Tg\,yr^{-1}$ with a total model diversity[1], δ, of 49% (Textor et al., 2006). The Ae-

[1]Total model diversity, δ, is computed as the standard deviation of the model values normalized by the all-models average and expressed as a percentage.

ACPD
9, 8469–8539, 2009

roCom GCMs estimate that wet removal accounts for 32% of total removal, though there is considerable variability between the models (δ=54%). The mean atmospheric residence times are on the order of 4 days (δ=43%) resulting in a mean estimate of global annual average aerosol dust burden of 20 Tg (δ=40%). AeroCom simulations of mineral dust indicate this aerosol accounts for ~70% of the global annual average dry aerosol mass. However, dust accounts for only 25% of global annually average aerosol optical depth (AOT), a value comparable in magnitude to hygroscopic aerosol such as sulfates and sea salt (Kinne, 2006). The recognition that anthropogenic secondary aerosol precursors (e.g. SO_2, NO_2 and HNO_3) can react with natural mineral aerosol, has led to several model studies designed to evaluate the effects of heterogeneous chemical reactions on aerosol direct and indirect effects (Bauer et al., 2007; Fan et al., 2004; Tang et al., 2004).

Heterogeneous reactions were found to increase wet deposition of dust near the Asian source regions resulting in up to a 50% decrease in deposition over the Eastern North Pacific (Fan et al., 2004). Citing Lammel and Novakov (1995) as well as Wyslouzil et al. (1994), Bauer et al. (2007) assumed dust particles with a 10% surface coating of sulfate or nitrate behaved as if they were completely soluble. The studies cited are hardly applicable to the formation of "soluble dust", as they investigated the coating of homogeneous, hydrophobic, primary soot with soluble sulfate and nitrate species. However, based on this assumption, Bauer et al. conclude that enhanced wet deposition of "soluble dust" leads to a 20% reduction (33.5 vs. 41.6 Tg) in the present-day global annual dust budget, compared to NASA GISS ModelE simulations that omit heterogeneous reactions.

Particles with diameters greater than ~2 μm activate regardless of composition for supersaturations typical of continental and marine cumulus cloud (~>0.2%) (Kelly et al., 2007). At 0.2% supersaturation $CaCO_3$ and SiO_2 with a 1% coating of gypsum, will activate if they have dry diameters greater than ~1 μm. Activation of "completely insoluble" dust particles in the 0.6–2.0 μm size range is facilitated by the presence of slightly soluble compounds (Kelly et al., 2007). These findings are supported by field

ACPD
9, 8469–8539, 2009

measurements (Matsuki et al., 2009) which show that calcite-containing particulate are likely acting as CCN. Note however that Matzuki et al. could not determine whether S and Cl coatings of Si-rich cloud drops enhanced their activation, or whether the Si-rich particles were coated due to their activation in cloud. SiO_2's low reactivity suggests activation in cloud. Additionally, Kelly et al. show that for dust-storm like conditions (high concentrations of "reacted" dust; low background aerosol concentrations), activating dust could be responsible for observations of rainfall suppression (Rosenfeld et al., 2001). Dust particles larger than $\sim 0.2\,\mu$m are all effective cirrus cloud ice nuclei (Archuleta et al., 2005), however recent laboratory studies show that heterogeneous reactions can inhibit the ice-nucleating ability of kaolinite under conditions found in the troposphere (Eastwood et al., 2009). Given the difficulty in simulating relative humidity (Petch, 2001) and aerosol indirect effects using GCM's (Penner et al., 2006), it is difficult to have confidence in recent model estimates of the influence of heterogeneous chemical reactions on atmospheric residence times of mineral dust.

Bauer et al. also calculate a 20% reduction in present-day dust burden compared to pre-industrial values (33.5 vs. 41.8 Tg) when heterogeneous chemical reactions are considered in both simulations. Present-day versus pre-industrial simulations should potentially include emissions of primary urban dust (Alfaro et al., 2003; Cohen et al., 2004), soil dust from agricultural activities (Sokolik and Toon, 1996; Tegen and Fung, 1995; Tegen et al., 2004), and dust emissions due to anthropogenically-induced desertification (Chen et al., 1999; Moulin and Chiapello, 2006; Sheehy, 1992). Furthermore, short model integration times (e.g. 6 years in Bauer et al.) cannot capture inter-decadal variability in precipitation and vegetative cover; which likely exerts a controlling influence on dust generation (Dai et al., 1997; Nicholson et al., 1998). The absence of dynamic aerosol size distributions with size resolved, and source-dependent, mineral compositions in GCM's mean that recent comparisons between pre-industrial versus contemporary dust burdens are likely an over-simplification.

The Chinese "Loess plateau" is the world's largest deposit of loess; a sedimentary deposit of wind blown silt- and clay-grade material. The loess-paleosol sequence of

the Loess plateau has a relatively continuous deposition character over the past 2.4–2.6 million years (Liu, 1985), with recent work potentially extending the geological time scale of its formation to ~7.0 million years (Ding et al., 2001). Electron microscope analysis of Chinese Loess show that the upper part of the stratigraphy is comprised of a meta-stable microfabric of plate-like aliminosilicates (~>70 wt%) (Derbyshire, 1983; Ding et al., 2001; Liu, 1985). The matrix is bound by calcium carbonate (calcite) and, occasionally, siliceous cement. Calcite associated with the Chinese Loess is in the medium to coarse, 6–60 μm, silt grains (Qizhong et al., 1964). While aluminosilicates and quartz grains are also a component of the silt-sized loess material, iron oxides are surface-bound to the clay grade (<6.0 μm) aluminosilicates. Free and surface adsorbed iron oxides account for ~3–6 w% (Liu, 1985) with a higher proportion of goethite:hematite (3:1) than African dusts (Lafon et al., 2006). Chinese loess contains a variable wt% of $CaCO_3$ (3.6–21%) with a mean value of 12 w% (Liu, 1985). Laboratory tests of water adsorption indicate no more than 3-4 monolayers of H_2O on the surface of these oxides under typical atmospheric conditions (Grassian, 2001) and references therein). HNO_3 and NO_2 will adsorb directly onto metal oxides (Al_2O_3, Fe_2O_3, TiO_2, CaO and MgO) of common minerals with the notable exception of SiO_2. The presence of adsorbed water greatly enhances the NO_2 and HNO_3 uptake coefficients compared to dry conditions. However reactions between NO_2 and HNO_3 with Al_2O_3, Fe_2O_3 and TiO_2 are surface limited, i.e. there is no reaction with internal crystal structure, whereas the reactions with CaO, MgO, and especially $CaCO_3$, occur throughout the bulk particle (Grassian, 2001).

Here we use in-situ airborne measurements of trace gases, aerosol microphysics and chemistry to evaluate the potential for heterogeneous chemical reactions between Asian pollution and Asian dust to influence aerosol optical properties over the Eastern North Pacific. We include an analysis of the heavily polluted continental boundary layer (CBL) and free troposphere (FT) near Mexico City as well as the results of long-term measurements at the Mauna Loa Observatory (MLO) in Hawaii. These results are then discussed with regard to modeling studies in order to evaluate model assumptions and

the plausibility of some of their conclusions regarding heterogeneous reactions occurring on dust particulate, their effects on aerosol optical properties, and the partitioning of nitrogen species between the gas and aerosol phases.

2 In-situ sampling of tropospheric aerosols during INTEX-B

During spring of 2006 the NASA DC-8 participated in Phase B of the Intercontinental Chemical Transport Experiment (INTEX-B), also a component of the Megacities Initiative: Local and Global Research Observations experiment (MILAGRO) (Molina et al., 2007; Singh et al., 2009). The NSF/NCAR C-130 participated in MILAGRO and the Pacific phase of INTEX-B with funding provided by the US National Science Foundation (NSF). During March of 2006 both aircraft were used to characterize the near-field trace gases and aerosols from the Central Mexican Plateau and their regional transport out over the Gulf of Mexico. During the last two weeks of April and the first two weeks of May 2006 the DC-8 was stationed in Honolulu, Hawaii and then Anchorage, Alaska while the NSF/NCAR C-130 was stationed in Seattle, Washington. During this period both aircraft sampled the marine boundary layer and free troposphere to study the long-range transport of Asian pollution and dust to the west coast of North America.

A detailed review of the meteorological setting during the measurements over Mexico can be found in Fast et al. (2007). The Hawaii phase of INTEX-B was climatologically average while the Alaskan phase of INTEX-B was climatologically "wet" with more frequent than average occurrence of low-pressure cyclonic weather systems in the North Pacific (H. Fuelberg, personal communication).

2.1 In-situ measurements of aerosol size distributions

Aboard the NASA DC-8 the University of Hawaii solid diffuser inlet (UH inlet) delivers ambient air to the combined NASA Langley Research Center (LaRC) and Hawaii Group for Environmental Aerosol Research (HiGEAR) aerosol sampling package. Sample air

ACPD
9, 8469–8539, 2009

is delivered to the University of New Hampshire's (UNH) filter-based aerosol chemistry system via the UNH solid diffuser inlet. Supermicrometer aerosol passing efficiencies were recently evaluated for these two inlets over the entire performance envelope of the NASA DC-8 (McNaughton et al., 2007). Aboard the NSF/NCAR C-130 sample air is delivered to the HiGEAR instrument package via a solid diffuser inlet evaluated during PELTI (Huebert et al., 2004).

Total and refractory (residence time, τ=0.1s @360°C) aerosol number ($Dp>$ 10 nm) are measured using two TSI model 3010 condensation nuclei counters (Clarke et al., 1997). Custom built differential mobility analyzers (DMA) are used to measure aerosol size distributions over the d_m=0.010–0.20 μm size range aboard both aircraft. The DMAs are equipped with a lagged aerosol grab sampler (LAG chamber) (Clarke et al., 1998). Each DMA system is also equipped with a heater assembly or, thermo-optical aerosol discriminator (TOAD), which pre-heats the aerosol to 150°C or 300°C (τ=0.2 s) prior to analysis (Clarke, 1991). In polluted airmasses the internally mixed refractory aerosol is commonly comprised of the "soot" components responsible for light absorption (Clarke et al., 2007, 2004; Mayol-Bracero et al., 2002). Preheating the aerosol does not affect the analysis of sea salt or dust, the most common natural refractory primary aerosol species. During INTEX-B the DC-8 aerosol package was equipped with an additional "long" DMA (LDMA, d_m=0.01–0.50 μm) and employed a smaller mini-LAG chamber but no TOAD. The MILAGRO C-130 did not contain an additional LDMA unit.

Both aircraft were equipped with a custom modified PMS LAS-X optical particle counter used to measure the aerosol size distribution between d_{oe}=0.1 and 20.0 μm at a size resolution of 112 channels per logarithmic decade. Each OPC is equipped with a 4-channel TOAD assembly operating at dry[2] ambient temperature, 150°C, 300°C and 420°C (τ=2.0 s) (Clarke et al., 2007). The OPC's are calibrated using monodisperse polystyrene spheres with a density of 1.05 g cm^{-3} and a refractive index of 1.59@589 nm. OPC sizing accuracy is also evaluated using borosilicate glass beads

[2]Ram heating plus 50% dilution with desiccated air.

with a density of 2.52 g cm^{-3} and a refractive index of 1.56@589 nm, and silicon dioxide (SiO_2) spheres with a density of 2.01 g cm^{-3} and a refractive index of 1.40@589 nm. The aerosol size determined by the OPC instrument are optically effective diameters (d_{oe}) as discussed in Clarke et al. (2004). During post-processing the unheated OPC size distributions are adjusted to d_g, to account for sizing errors due to aerosol refractive indices that differ from those of the PSL calibration spheres (1.59@589 nm). OPC sizes over the 0.12–0.53 μm size range are adjusted assuming an ammonium sulfate composition with a refractive index of 1.53-0.0i. When sampling mineral dust the OPC sizes over the size range 0.53–8.0 μm are adjusted assuming a refractive index of 1.53–0.0006i. When sampling sea salt aerosol no size adjustment is made to the data in the 0.53–8.0 μm size range because the dry sea salt refractive index (1.588-0.0i) is close to that of PSL (1.59-0.0i) at the He-Ne laser wavelength of 633 nm. No optical to geometric size adjustments are made for the heated OPC channels as information regarding chemical composition, and thus refractive index, is a relative unknown. Since counting statistics and sizing accuracy of the OPC and UH solid diffuser inlet passing efficiency are poor beyond 8.0 μm, data above this size range is typically eliminated from the data sets.

Aerodynamic aerosol size distributions in the d_{ae}=0.5–20.0 μm size range are measured using a TSI model 3321 aerodynamic particle sizer (APS). APS flow and sizing calibrations were routinely performed according to the procedures outlined in McNaughton et al. (2007). Data from the first five channels (0.50–0.78 μm) were discarded due to poor instrument performance over this size range. Ignoring slip correction factors ($C_{c,ae}/C_{c,g}$) by approximating them as unity, aerodynamic diameters (d_{ae}) were adjusted to geometric diameters (d_g) during post processing (Baron and Willeke, 2001; DeCarlo et al., 2004). We assume a dry bulk density of 2.06 g cm^{-3} for Chinese loess (Liu, 1985). This bulk density is used to correct supermicrometer mineral aerosol aerodynamic to geometric diameters and when converting aerosol volume to mass and vice versa. This is equivalent to assigning a shape factor, χ, of 1.10–1.25 for dust particles with aerodynamic diameters between 0.5 and 10.0 μm assuming a bulk

density for crustal material of 2.56 g cm^{-3} (Craig, 1997). The loess value (2.06 g cm^{-3}) is nearly identical to the "effective density" of 2.0 g cm^{-3} proposed by Reid et al. (2003) but smaller than the value used in McNaughton et al. (2007) to evaluate DC-8 inlet passing efficiencies. When recalculated, the 50% passing efficiency diameters of the UH and UNH inlets are no less than 3.5 μm and 2.8 μm when sampling Asian dust at the surface and 2.2 μm and 1.8 μm when sampling at the DC-8 ceiling of 12 km.

2.2 In-situ measurements of aerosol optical properties

Total aerosol light scattering is measured aboard each aircraft using TSI model 3563, 3-wavelength (3-λ) integrating nephelometers (TSI-Neph) (Anderson et al., 1996; Anderson and Ogren, 1998). Submicrometer aerosol light scattering is measured using Radiance Research model 903 single-wavelength nephelometers (RR-Neph). The Anderson and Ogren (1998) truncation correction has been applied to the TSI-Neph data while the empirically derived truncation correction of Anderson et al. (2003) has been applied to the RR Neph data. Calibrations using filtered CO_2 and Refrigerant 134A were performed prior to each deployment and every 3–5 flights. No significant (<5%) calibration adjustments were required for the TSI-Nephs while slight (5–10%) adjustments were often required for the zero and span of the RR-Nephs. During each flight at least one 300-s filtered air sample was collected to check for leaks and/or deviations from zero. Accuracy (±2%) and precision (0.2 Mm^{-1} for 300 s average) estimates for these instruments are comparable to those determined previously (Anderson et al., 2003; Anderson and Ogren, 1998).

Total and submicrometer aerosol absorption is measured using 3-λ PSAP's corrected according to Virkkula et al. (2005). In laboratory tests prior to the MILAGRO and INTEX-B experiment three of the four 3-λ PSAPs were tested for instrument noise while sampling filtered air. The average instrument noise (δ_{300}) is computed as the average standard deviation for six, 300 s (5-min) averages of the 1-Hz data (Table 1). These values are comparable to instrument noise (δ_{240}=0.72 Mm^{-1} and 0.33 Mm^{-1})

reported for the single-wavelength PSAPs used to measure total and submicrometer absorption during ACE-Asia (Anderson et al., 2003). PSAP #4 was not delivered from the manufacturer until after the November 2005 intercomparison. Note that while instrument noise and thus precision of the PSAP's can be assessed, we have no way to calibrate the instruments for absolute accuracy. During MILAGRO and INTEX-B there were three intercomparison flights where the NASA DC-8 and the NSF/NCAR C-130 flew in formation. Total and submicrometer aerosol absorption was comparable during these time periods (not shown). Small discrepancies due to flow rate calibrations and errors in filter spot sizes have been corrected.

Two RR-Nephs are used to measure aerosol f(RH) between 80% and 40% RH at a wavelength of 532 nm. Air sampled by one nephelometer (RRwet) is preconditioned to a relative humidity of 80%±7% using a custom designed f(RH) system employing a GORE-TEX^{TM} membrane. The second nephelometer (RRdry) was plumbed in parallel and outfitted with a commercial blanket heater. The blanket heater raises the nephelometer temperature by 5–10°C reducing the relative humidity to values below 40% in the humid (RH_{amb}>90%) marine boundary layer and often below 5% in the free troposphere. This heating may cause minor evaporation of non-refractory species of the order of a several percent of the mass of organic species and ammonium nitrate (Huffman et al., 2008). Using the corrected scattering values and RH recorded by the RRdry and RRwet nephelometers, a two point fit is used to compute γ, the exponential term in the f(RH) equation:

$$\sigma_{sp,amb} = \sigma_{sp,dry} \cdot \left(\frac{1 - \frac{RH_{dry}}{100}}{1 - \frac{RH_{amb}}{100}} \right)^{\gamma} \quad (1)$$

where, $\sigma_{sp,dry}$ and $\sigma_{sp,amb}$ are light scattering at the indicated "dry" and "ambient" relative humidities (Carrico et al., 2003; Howell et al., 2006).

A ground-based test of the f(RH) system was performed in its flight configuration aboard the NASA DC-8. The results indicate that scattering measurements for ammonium sulfate and sea salt (from a filtered North Pacific subtropical gyre seawater

standard (Karl and Lukas, 1996)) are within 25% of the values calculated from size distributions calculated for salt densities and optical properties at 80% relative humidity (Tang, 1997; Tang and Munkelwitz, 1994; Tang et al., 1997). Since f(RH) is computed from a two point fit of the ratio between the dry and wet scattering values the f(RH) measurement could be low by up to a factor of 0.7 or overestimated by up to a factor of 1.3.

2.3 Fitting aerosol size distributions using lognormal distributions

In this analysis, DMA, OPC and APS size distributions are averaged, combined, then fit using log-normal distributions (Baron and Willeke, 2001; Seinfeld and Pandis, 1998). Other researchers have applied log-normal fitting routines using least squares optimization (Hand and Kreidenweis, 2002; Osborne and Haywood, 2005; Porter and Clarke, 1997). However, in the cases cited only one moment of the aerosol size distribution is considered during the fit. When fitting the number distribution (Osborne and Haywood, 2005; Porter and Clarke, 1997) the tail of the distribution does not significantly contribute to the least squares error. But, the tail of the number distribution contains all of the aerosol volume and will be poorly constrained by fitting the distribution using only aerosol number. Similarly, when fitting using the volume distribution (Hand and Kreidenweis, 2002) aerosol number will be poorly fit.

To avoid the problems associated with fitting a single mode of the distribution, we (S. Howell) developed a least squares fitting routine which simultaneously evaluates the least squares error for the number, length, area and volume distributions (i.e. the zeroth through third moments). This technique is similar to that of Stroud et al. (2007), who simultaneously fit the number and volume distribution from an SMPS and the species mass distributions from an AMS. Using multiple moments results in better fits, which do not bias the results by large errors contributed from a single mode. Typically, one to three modes (termed the Aitken, accumulation and coarse modes), were required to fit the unheated distributions. In general only two fits, Aikten and coarse mode, are required to fit the refractory aerosol distributions. As indicated in our previous

studies (Clarke et al., 2007, 2004), the refractory Aitken mode aerosol is found to be an internally mixed component of some fraction of the unheated accumulation mode aerosol.

2.4 Aerosol chemistry measurements

Aboard the NASA DC-8 the University of New Hampshire collects total aerosol filters with 300–600 s resolution, measuring Na^+, NH_4^+, K^+, Mg^{2+}, Ca^{2+}, Cl^-, NO_3^-, SO_4^{2-}, and $C_2O_4^{2-}$ using ion chromatography (Dibb et al., 2003b). Measurements of ^7Be are performed using gamma-spectroscopy (Dibb et al., 1997). Fast (90-s) measurements of HNO_3 (g) and fine aerosol SO_4^{2-} are measured using ion-chromotography coupled to a mist chamber (Scheuer et al., 2003). Aboard the NSF/NCAR C-130, the University of Colorado measured submicrometer non-refractory aerosol chemistry (NH_4^+, NO_3^-, SO_4^{2-}, NR Cl^-, and organics) using a high-resolution time-of-flight aerosol mass spectrometer (HR-ToF-AMS) (Canagaratna et al., 2007; DeCarlo et al., 2008, 2006; Dunlea et al., 2008). The HR-ToF-AMS data are recorded as 10 s. averages and further averaged into 60-s samples.

2.5 Trace gas measurements

DC-8 trace gas measurements of NO_2, HNO_3, total peroxynitrates (PNs), alkyl- and hydroxyalkyl nitrates (ANs) were measured by the University of California, Berkeley using thermal-dissociation coupled to laser-induced fluorescence (TD-LIF) (Day et al., 2002; Thornton et al., 2000). Based on previous studies (Miyazaki et al., 2005; Zondlo et al., 2003) and recent measurements during ARCTAS (P. Wennberg, personal communication), it is likely that the UC Berkeley TD-LIF and UNH DC-8 mist chamber measurements of HNO_3 include a 10–30% enhancement due to contamination by NH_4NO_3 aerosol, with larger enhancements possible in the presence of dust (Miyazaki et al., 2005). For INTEX-B the two HNO_3 measurements are highly correlated over more than 2 orders of magnitude (m=0.89, R^2=0.83) and are averaged to produce a single

measure of HNO_3. No attempt has been made to correct the HNO_3 data for particulate nitrate contamination. SO_2 was measured by the Georgia Institute of Technology chemical ionization mass spectrometer (Kim et al., 2007). NO was measured using chemiluminescence (Sjostedt et al., 2007). Ozone was measured using nitric oxide chemiluminescence by the NASA Langley Research Center (Davis et al., 2003).

Aboard the NSF/NCAR C-130, HNO_3 was measured by the California Institute of Technology using a chemical ionization mass spectrometer (Crounse et al., 2006). NO, NO_2, NO_y, and O_3 were measured by a team from the National Center for Atmospheric Research (NCAR) using a 1-Hz chemiluminescence technique (Weinheimer et al., 1998). PAN was measured by an NCAR team using thermal decomposition chemical ionization spectrometry (Slusher et al., 2004).

3 Results

3.1 Anthropogenic pollution and Asian dust over the Eastern North Pacific

DC-8 data from the Pacific Phase of INTEX-B is stratified into data collected near Hawaii (Latitude <40° N) and Alaska (Latitude >40° N). The locations correspond to the climatological features known as the East Pacific High and the Aleutian Low. Sampling was conducted between 15 April and 1 May 2006 near Hawaii and between 1 and 15 May, near Alaska. The free troposphere (GPS altitudes >1.5 km) during this time was widely influenced by Asian pollution as well as Asian dust (Dunlea et al., 2008; Singh et al., 2009). After excluding clean FT airmasses (CO<90 ppbv; O_3<40 ppbv), and those indicative of stratospheric influence (^{7}Be>800 fCi sm^{-3}, where sm^{-3} denotes concentrations per cubic meter of air at 1013.25 mb and 273.15 K), the data were further stratified using the fine mode fraction of aerosol light scattering (Anderson et al., 2003).

$$\mathrm{FMF}_{\mathrm{scat}} = \frac{\sigma_{\mathrm{sp},550,\mathrm{Dae}<1.0}}{\sigma_{\mathrm{sp},550}} \quad (2)$$

ACPD
9, 8469–8539, 2009

When $FMF_{scat} > 0.6$, and scattering exceeded $3\,Mm^{-1}$, the airmasses are considered "fine" mode dominated anthropogenic pollution. Values of $0.3<FMF_{scat}<0.6$ are labeled "mixed" pollution and mineral dust. No data met the "dusty" $FMF_{scat}<0.3$ criteria of Anderson et al. (2003).

Lognormal fits of the anthropogenic and mixed aerosol size distributions measured near Hawaii are presented in Fig. 1. The top two panels are the number and volume distributions for the fine mode dominated case whereas the bottom panels are for the mixed airmass type. Differences between the unheated and refractory fits to the supermicrometer dust mode are not significant and the summary statistics in Table 2 are pooled into a single supermicrometer aerosol fit. Figure 2 assesses the degree of aerosol number closure by comparing the integrals of the lognormal fits to the average concentrations measured using the hot and cold CN counters (N for $Dp>10\,nm$ sampled at 1-Hz). Size distribution integrals reasonably replicate the faster CN counter averages and support the use of these fits to constrain model simulations of the aerosol size distribution. Figures 3 and 4 are the fits and the number closure assessment for the data collected in the FT of the Aleutian Low. For these cases refractory number is somewhat higher in the fit data resulting in fair agreement between the RCN ratios.

Table 2 summarizes the mean log-normal fits to the accumulation mode, coarse mode and refractory Aitken mode size distributions measured near Hawaii and Alaska for the fine mode dominated and mixed airmass types. After long range transport, the number median diameter (NMD) of FT Asian pollution ($FMF_{scat}>0.6$) aerosol varies (± 1-σ) between 0.086 and $0.15\,\mu m$ with an average value of $0.11\,\mu m$ and a geometric standard deviation, σ_g, of 1.70 ± 0.15. The observed range (± 1-σ) of volume median diameters (VMD) is between 0.24 and $0.30\,\mu m$. In the presence of dust ($0.3<FMF_{scat}<0.6$), the NMD of FT Asian aerosol varies between 0.051–$0.11\,\mu m$ with a smaller average NMD of $0.075\,\mu m$. In the presence of dust the accumulation mode aerosol has a broader distribution, $\sigma_g=1.97\pm0.20$, which results in a range of VMD's between 0.26 and $0.35\,\mu m$. Despite their larger VMD's, for a fixed number of particles, the average value of the fit to the "mixed" aerosol types result in 30% less aerosol vol-

ume than under low-dust conditions. This is close to the significant difference (α=0.05) of 40% between the average accumulation mode volumes for the observed distributions (V_{anthro}=1.4±1.5 $\mu m^3\,cm^{-3}$; V_{dusty}=0.86±0.64 $\mu m^3\,cm^{-3}$); a quantity that will vary due to factors such as emissions source strength, transport pathway etc.

The total and refractory number distributions highlight the internally mixed nature of the refractory soot particulates coated with the non-refractory compounds, NH_4^+, SO_4^{2-}, NO_3^- and organics. The ratio of refractory number to total number in these airmasses averages 0.75 indicating only 25% of the pollution aerosol is composed of externally mixed secondary aerosol number. The refractory aerosol NMD's for Hawaii and Alaska vary between 0.032 and 0.066 μm with a mean value of 0.046 μm. The geometric standard deviation is variable but averages 1.91±0.23. This results in a range of VMD's between 0.10 and 0.26 μm for the refractory material. The average refractory volume ratio of the log normal fits is 14–19%, in good agreement with the observed average refractory volume ratios of 12–16%±7%. The INTEX-B observations of reductions in accumulation mode secondary aerosol mass due to competition by dust surface area is consistent with previous observations near the Asian source region (Howell et al., 2006). Models which attempt to simulate these aerosol should account for this internal mixing as surface coatings of non-absorbing secondary aerosol on internally mixed carbonaceous primary aerosol will affect aerosol optical properties (Clarke et al., 2004; Fuller et al., 1999; Schnaiter et al., 2005).

Total aerosol single scatter albedo (SSA) at 550 nm measured 0.94±0.03 and 0.95±0.01 for fine mode dominated (FMF_{scat}>0.6) airmasses sampled near Hawaii and Alaska. Using a one-tailed Student's t-test these values are significantly higher than the value of 0.90±0.02 measured near the East Asian source region during ACE-Asia (Anderson et al., 2003). The INTEX-B and ACE-Asia measurements use the same instrumentation with comparable levels of uncertainty. The only difference is the use of the Virkkula et al. (2005) PSAP correction for these data rather than the Bond et al. (1999) correction for ACE-Asia. The correction factor does not significantly alter the means indicating an increase in SSA during long-range transport of Asian pollution

ACPD
9, 8469–8539, 2009

across the Pacific. The 550 nm SSA's for mixed airmasses ($0.3<FMF_{scat}<0.6$) measured near Hawaii and Alaska have values of 0.96 and 0.97 (±0.02), significantly different than the 0.91 (±0.02) measured near East Asia. The SSA's at 450 and 700 nm are included in Table 3 along with the values measured in the continental boundary layer over the Central Mexican Plateau and the FT and MBL over the Gulf of Mexico.

Measurements of 3-λ total aerosol scattering and absorption allow us to investigate the wavelength dependence of extinction for Asian aerosol after long-range transport to the remote North Pacific. Table 3 summarizes the total scattering Ångstrom exponent as well as the total absorption Ångstrom exponents measured for the fine mode dominated and mixed aerosols. The averages are computed from 5-min level leg FT averages where the measured absorption is above 0.1 Mm^{-1}. Values from the Central Mexican Plateau and the FT over the Gulf of Mexico are also included for comparison. The Hawaii data show the lowest scattering Ångstrom exponents (i.e. the most dust) and the highest absorption Ångstrom exponents. Data from Mexico and Alaska are more comparable for both the fine mode dominated and the mixed aerosol.

Submicrometer absorption Ångstrom exponents are always higher when dust is present (not shown). The f(RH) measurements (Table 4) also show that submicrometer f(RH) γ is suppressed (0.39–0.44) in the presence of dust when compared to fine-mode dominated values of γ (0.44–0.50). These two measurements indicate that a portion of the dust is passing the 1.0 μm aerodynamic (at STP) cut-off of the impactor plate. Ignoring shape factor, the impactor's 50% cut corresponds to a geometric diameter of 0.67 μm for a mineral dust aerosol with a density of 2.06 g cm^{-3}. Based on the lognormal fit for the Hawaii mixed aerosol data (N=5.3 cm^{-3}, NMD=0.64 μm, σ_g=2.06), this "submicrometer" dust is 0.3 $\mu g\, m^{-3}$ of the total, 15.7 $\mu g\, m^{-3}$. Using a refractive index of 1.53-0.0006i, the "submicrometer" tail of the dust distribution, which accounts for just 2% of the dust mass, accounts for 11% of the extinction by mineral dust.

Poorly modeling the lower tail of the mineral aerosol size distribution (2% of dust mass) can result in larger errors in aerosol extinction (11% of dust extinction at 550 nm). As shown by the wavelength dependence measurements, this error will compound

ACPD
9, 8469–8539, 2009

when calculating extinction at shorter visible wavelengths and in the UV (Sokolik and Toon, 1999) as well as for dusts with differing composition (e.g. Lafon et al., 2006). For the Hawaii example, dust number below dg=1.0 μm represent 72% of the total number and may not activate at low supersaturations (~<0.2%) without first undergoing heterogeneous reactions (Kelly et al., 2007). Thus accurately modeling the direct and indirect effects of mineral dust likely requires dynamic aerosol size distributions with size resolved, and source-dependent, mineral composition.

3.2 Heterogeneous chemistry of Asian dust over the Eastern North Pacific

The previous section demonstrated that Asian pollution and dust commonly occur together in polluted airmasses transported long-range across the Pacific. In this subsection we examine the chemistry of accumulation mode and coarse mode aerosol measured in the pollution/dust plumes over the Eastern North Pacific. University of New Hampshire filter-based measurements of Ca^{2+} can be converted into calcite ($CaCO_3$) mass assuming that the weak-acid eluent of the UNH ion chromatography analysis does not measure the aluminosilicate's structural calcium. When these values are regressed against the HiGEAR data (Fig. 5) we estimate a calcite content of 11 wt% for the Hawaii region (R^2=0.90) and 10 wt% (R^2=0.57) for the Alaska region. The low R^2 of the Alaskan fit is being driven by the two highest values of aerosol Ca^{2+}. A calcite weight percent of 10–11% is in close agreement with the range of calcite wt%'s reported for the Chinese Loess parent material; 3.6–21% with a mean value of 12% (Liu, 1985).

The ratio of sulfate aerosol to the sum of gas phase SO_2 plus sulfate aerosol (S-ratio) has been shown to increase with airmass age in previous studies (Brock et al., 2008; Dunlea et al., 2008). Values greater than ~0.5 generally indicate airmass ages greater than ~3 days, although lower values can be observed in older airmasses after wet deposition. In the presence of the dust we can expect heterogeneous reactions to drive the S-ratio toward unity at a faster rate. Jordan et al. (2003a) evaluated the ratio of particulate nitrate (NO_3^-) to nitrate plus nitric acid (N-ratio) in order to evaluate

the heterogeneous uptake of NO_x species by alkaline dust. Their observations show that in the presence of dust, particulate nitrate accounts for 50–60% of total nitrate. The values range between 25% and 50% without dust. Figure 6 plots both the S-ratio and the N-ratio versus calcium measured between Hawaii and Alaska during INTEX-B. The plots are color coded by scattering Ångstrom exponent, high values (red) indicative of small particles found in pollution dominated airmasses and low values (blue) indicative of airmasses whose optical properties are dominated by supermicrometer dust. For the S-ratio (left-panel) there is no clear dependence with calcium concentration. This indicates that airmass age and/or scavenging could control the partitioning of sulfur. The N-ratio versus Ca^{2+} plot (middle) shows that for low Ca^{2+} concentrations (<200 pptv) the ratio averages 47% (±22%) and that at higher concentrations (>200 pptv) the value averages 65% (±25%), a significant difference using a two-tailed Student's t-test (α=0.05). It is also interesting to note that both the low-Ca^{2+} and high-Ca^{2+} cases from INTEX-B have values higher than the near-source Jordan et al. values. This implies that heterogeneous reactions continue to take place during long-range transport. The effect of these reactions is even more striking when aerosol nitrate is divided by the sum of all nitrogen species (NO, NO_2, HNO_3, PAN, ANs, PNs, and NO_3^-). The presence of dust is clearly sequestering gas-phase nitrogen species into the particulate-phase (Fig. 6 – right). Aerosol nitrate accounts for only 10% (±6%) of the nitrate in the low dust group (<200 pptv Ca^{2+}) whereas it averages 26% (±11%) in the high dust group and has maximum values approaching 50%.

These reactions are explored further in Fig. 7 where we plot aerosol SO_4^{2-} (top-left) and NO_3^- (bottom-left) in neq sm^{-3} (T=273.15 K, P=101.325 kPa) versus the equivalents of Ca^{2+}. The regression for sulfate is poor but can be improved, with a slope of 0.16 and intercept near zero, by subtracting the submicrometer sulfate. And although Chinese Loess is not rich in $CaSO_4$ (Liu, 1985). Arimoto et al. (2004) reported an SO_4^{2-} to WS Ca^{2+} molar ratio of 0.09±0.04 for clean (North Winds), dust dominated (>40 $\mu g\,m^{-3}$) aerosols at Zhenbeitai, China during ACE-Asia. A ratio of 0.1 is also the minimum value measured by Kline et al. (2004) aboard the NSF/NCAR C-130 during

ACE-Asia. The poor fit to the INTEX-B data (R^2=0.215) means we cannot rule out the possible presence of gypsum.

The regression for nitrate indicates a close coupling between the presence of aerosol nitrate and mineral dust (m=0.13, R^2=0.69). Primary $Ca(NO_3)_2$ can likely be ruled out as Arimoto et al., reported a molar equivalents ratio of NO_3^-/WS Ca^{2+} of just 0.008. Plotting the degree of aerosol neutralization against equivalents of calcium (middle of Fig. 7) and coloring the data by scattering Ångstrom exponent shows that there is generally sufficient ammonium to neutralize most SO_4^{2-} to form $(NH_4)_2SO_4$. Also, there is generally insufficient ammonium to create much NH_4NO_3. Using the method of Jordan et al. (2003a) we plot excess sulfate and excess sulfate plus nitrate, i.e. equivalents of SO_4^{2-} and NO_3^- which cannot be paired with available NH_4^+, versus aerosol calcium in the right panels of Fig. 7. The data are accompanied by the 1:1 alkalinity line (blue), the regression from Jordan et al. (red), and a linear regression for the INTEX-B data (black). Note that the Jordan et al. regressions were for near source Ca^{2+} values that ranged from 100–1000 neq sm^{-3} whereas the INTEX-B concentrations are substantially reduced (max~120 neq sm^{-3}) likely due to removal processes (Dunlea et al., 2008), as well as dilution during long-range transport. The regression for the sum of excess sulfate and nitrate versus calcium is slightly more significant (R^2=0.30) than that for sulfate alone (R^2=0.12) but both results are less robust than the regression of sulfate and nitrate to calcium directly. While there is the potential that these species are simply co-emitted at the source, this could also indicate that the Jordan et al. assumption that all ammonium is associated with submicrometer sulfate or nitrate is inaccurate. Furthermore, when combined with the potential influence of submicrometer calcium-containing particulate of anthropogenic origin (e.g. fly ash), the inherent uncertainty in airborne measurements of supermicrometer aerosol (Blomquist et al., 2001; Huebert et al., 2004; McNaughton et al., 2007) as well as ammonium nitrate (Bergin et al., 1997), it is not surprising that these regressions are not very robust. Still, the trend, especially for nitrate, suggests 6–17% of the calcium's alkalinity has been consumed by acidic nitrogen species that, in the absence of dust, may have remained in the gas

phase or in the submicron particle mode.

For this irreversible reaction to account for the increase in aerosol nitrate we need to establish whether or not the Ca^{2+} measured in the Asian plumes is actually calcite. We have already used the size distribution measurements to derive an 11 wt% of $CaCO_3$ for the dust aerosol (Fig. 5). The variability of the calcite wt% in Chinese Loess (3.6–21%; Liu, 1985) leaves a relatively large margin for error and the 11 wt% reported here is higher than the near source values (5–8 wt%) reported by Kline et al. (2004). The left panel of Fig. 8 plots the anions versus cations for the UNH filter-based chemistry measurements. Minor cations such as Fe^{2+} are not measured by the UNH IC technique but their concentrations are expected to be a small fraction of the total. Similarly H^+ is not reported thus the pH of the aerosol is unknown. The major missing anion in the analysis is CO_3^{2-}. Where a large anion/cation imbalance occurs we can assess the probability that the missing ion is CO_3^{2-} by plotting the imbalance vs. Ca^{2+} (center panel of Fig. 8). A slope of 1:1 would account for carbonate as calcite. Dolomite, $CaMg(CO_3)_2$, can also be a source of carbonate ions thus we also include a plot versus the sum of the molar equivalents of Ca^{2+}+Mg^{2+}. For both the Hawaii and Alaska data, large ion imbalances occur up to ratios of 1:4. When plotted vs. calcium the imbalance is reduced to within +15%. When plotted vs. the sum of the calcium and magnesium the imbalance is reduced to within −15%. This ±15% uncertainty can be considered the limit of the technique as a result of missing minor ions such as Fe^{2+} and H^+ and we conclude that the missing anion is most likely CO_3^{2-}.

3.3 Heterogeneous chemistry of Asian dust near the tropopause

Some tropospheric airmasses sampled during INTEX-B contained mineral dust as well as high concentrations (>800 fCi sm^{-3}) of the stratospheric airmass tracer ^{7}Be (Dibb et al., 2003a; Jordan et al., 2003b). Stratospheric concentrations of HNO_3(g) are typically higher than those observed in the FT. As a result, Asian dust lofted beyond the tropopause or into a FT airmass that mixes with stratospheric air could po-

tentially be re-exposed to nitric acid. This would result in additional conversion of $HNO_3(g) \rightarrow Ca(NO_3)_2$ in excess of the nitrogen species converted from the emission of anthropogenic precursors (i.e. NO_x). Adopting the same selection criteria and replicating the analyses described in the previous section, Fig. 9 (bottom-left) shows that nitrate is highly correlated (R^2=0.78) with Ca^{2+}. The data indicate 60% (±12%) of the nitrate resides in the aerosol phase at high dust concentrations (Ca^{2+}>200 pptv). The ratio of aerosol nitrate to the sum of all nitrogen species for the high dust cases is 24% (±13%), significantly different than the 6.9% (±5.1%) for the low Ca^{2+} data.

It is interesting to note that there is effectively no correlation between supermicrometer sulfate and calcium in the upper troposphere/lower stratosphere (UT/LS) samples (top left – Fig. 9). Also, there is generally excess ammonium ($NH_4^+/2{*}SO_4^{2-}$>1.0) to sulfate in these samples (top-center – Fig. 9). On the other hand, there is generally insufficient NH_4^+ to neutralize the measured sulfate plus nitrate concentrations ($NH_4^+/[2{*}SO_4^{2-}+NO_3^-]$<1.0) (bottom-center, Fig. 9). The result is a strong correlation between nitrate and calcium (R^2=0.78), and a fair correlation between excess sulfate plus nitrate and calcium (R^2=0.39). For the UT/LS samples the data indicate that 20–25% of the mineral aerosol alkalinity has been consumed by heterogeneous reactions. Once again there is a cation-anion imbalance (Fig. 10). This imbalance can be closed to within ±15% by assuming the missing anion is CO_3^{2-} initially present as calcite or dolomite; a fraction of which (20–25%) has reacted to form $Ca(NO_3)_2$. Note that the excess nitrate slope is higher (0.24 versus 0.17) compared to that of the other FT data (bottom-right, Fig. 7). Nitric acid concentrations are in the UT/LS airmasses are also higher, ~350 pptv, compared to 70–140 pptv for the HI and AK airmasses in the FT. However, when excess sulfate plus nitrate is plotted against ^7Be (not shown), there is no clear trend between elevated excess NO_3^- and ^7Be. Thus the higher slope and more robust correlation for the dust aerosol in UT/LS airmasses cannot be attributed directly to secondary exposure to stratospheric nitric acid. Possible explanations include higher initial concentration of anthropogenic NO_x mixing with the Asian dust near the source, and/or differing thermodynamic histories for the airmasses, including exposure to high

ACPD
9, 8469–8539, 2009

RH etc. The results do not preclude the possibility that exposure to stratospheric nitric acid can cause a second set of heterogeneous reactions to take place, but simply that this potential contribution cannot be determined from the INTEX-B measurements.

3.4 Heterogeneous chemistry in the nitrate-rich boundary layer of the Central Mexican Plateau

The Mexico City airshed is a complex setting with diverse sources of primary aerosol (soot, organics, dust) as well as secondary aerosol precursors (SO_2, NO_x, VOC's) (DeCarlo et al., 2008; Molina et al., 2007; Salcedo et al., 2006). A detailed analysis of aerosol in the airshed is beyond the scope of this publication. But, motivated by the success of the heterogeneous chemistry analysis over the remote Pacific, we evaluate the nitrogen rich boundary layer of the Central Mexican Plateau (alt <2.0 km a.g.l.), and the FT over the Gulf of Mexico (alt>1.5 a.g.l.), locations where the DC-8 measured the highest concentrations of mineral dust during MILAGRO/INTEX-B.

The left column of Fig. 11 are from the DC-8 dataset and indicate a poor correlation between sulfate and calcium due to a low calcium data cluster. The intercept for the regression can be brought to near zero by subtracting submicrometer sulfate, however, the trend with calcium is still not compelling evidence of heterogeneous reactions. The relationship between NO_3^- and Ca^{2+} is highly variable but a general trend is evident. There is generally sufficient ammonium to neutralize all of the sulfate aerosol. This is consistent with results in and around Mexico City where the submicron mode was almost always neutralized by ammonium (Aiken, 2009; DeCarlo et al., 2008; Salcedo et al., 2006). In some cases an excess of ammonium (middle – Fig. 11) can be seen as, e.g. in the large negative values for excess SO_4^{2-} shown in the upper-right panel of Fig. 11. Some of these data are associated with relatively fresh fire plumes sampled near Mexico City. After computing excess nitrate, there is sufficient ammonium to form both $(NH_4)_2SO_4$ and NH_4NO_3, but insufficient ammonium to consume all the excess acids. The excess sulfate plus nitrate plot (lower-right) is nearly identical to the near source values in Asia (Jordan et al., 2003a) and the somewhat robust (R^2=0.42)

correlation is indicative of heterogeneous reactions. The dust composition is a relative unknown, though ratios of Na:Ca and Mg:Ca are mostly indicative of crustal material rather than sea salt (not shown). The exceptions stand out as the large cation-anion imbalances that do not lie along the 1:1 line in the central and right panels of Fig. 12. These data points have geochemical ratios nearer to sea-salt and likely contain primary salts derived from dry lake beds of the Central Plateau which, were observed (CM^C) to be dust sources from on board the aircraft during the field campaign.

3.5 1996–2006 record of aerosol chemistry at Mauna Loa Observatory

Airborne data collected from a single campaign is effectively a point measurement in both space and time. Here we put the INTEX-B measurements into a broader temporal context by comparing the data to the long-term record from the Mauna Loa Observatory. For the past 12 years the University of Hawaii, has conducted long-term measurements of aerosol chemistry at the Mauna Loa Observatory (MLO) (Huebert et al., 2001). Figure 13 plots the neutralization of sulfate (left) and sulfate plus nitrate (right) as a function of aerosol calcium for the 11-year MLO record. When data with $[Ca^{2+}]$<25 pptv (0.05 $\mu g\,sm^{-3}$) are omitted, and the remainder are colour coded by scattering Ångstrom exponent, there appear to be two branches of dust data. The upper group corresponds to a neutralization ratio ~0.5 indicating a composition of close to ammonium bisulfate NH_4HSO_4. The lower branch of data has an equivalents ratio of ~0.2 indicating insufficient ammonium to react with the available sulfate. When the long-term MLO data are instead plotted as excess sulfate versus aerosol calcium and excess sulfate plus nitrate versus calcium, the coupling to alkaline dust becomes more clear (Fig. 14). Based on the regressions, excess sulfate has consumed ~16%, of the $CaCO_3$. The slope of the regression for the sum of excess sulfate plus nitrate is 1:0.30 indicating a further consumption of ~14% of the $CaCO_3$ by excess nitrate. Figure 14 also shows a number of low-dust cases (Ca^{2+}<20 neq sm^{-3}; <0.4 $\mu g\,sm^{-3}$) above the 1:1 alkalinity line. It is these instances where the buffering capacity of the Ca^{2+} as $CaCO_3$ could have been be exceeded and acid processing of the mineral dust is more

likely to have occurred (Solomon et al., 2009).

4 Discussion

4.1 The effect of heterogeneous reactions on Asian dust optical properties

In Fig. 15 we plot the range of mass (volume) distributions for dust (mean $\pm 1\,\sigma$, in blue and green) measured over the Eastern North Pacific during INTEX-B, as well as a Saharan distribution (red) measured after long-range transport (Maring et al., 2003). The hygroscopic growth factor for $CaSO_4$ and $Ca(NO_3)_2$ at 90% RH compared to 40% RH is a factor of ~1.5. Fully consuming 20 wt% of CaO, MgO and $CaCO_3$ to produce $CaSO_4$ or $Ca(NO_3)_2$ would only increase the volumetric mean diameter of the dust distribution from 2.5 μm to ~3.0 μm between these two RH's. Computing scattering at 550 nm assuming spherical particles and using Mie theory with a fixed refractive index (1.53-0.0006*i* (Clarke et al., 2004), shown in Fig. 15b), results in a 7–8% reduction in light scattering due to a reduction in mass scattering efficiency at larger sizes. This small difference in optical properties is negligible compared to the observed variability in the dust distributions and their composition. Additionally, this change in optical properties is small compared to the uncertainty in predicting ambient RH in climate models (Petch, 2001).

4.2 The effect of heterogeneous reactions on pollution aerosol optical properties

In the previous section we demonstrate that heterogeneous reactions have a negligible effect on dust optical properties. However, the presence of supermicrometer dust reduces the mass of secondary aerosol species that condense on primary aerosol of anthropogenic origin; a process that is approximately proportional to aerosol surface area (Howell et al., 2006). This significantly reduces the single scattering albedo of

ACPD
9, 8469–8539, 2009

the accumulation mode aerosol (Clarke et al., 2004) as well as f(RH) (Howell et al., 2006). Here we compare the reduction in ambient light scattering due to a reduction in accumulation mode NMD, to the effect of enriching the accumulation mode in relatively hydrophobic organic species, i.e. a reduction in non-refractory (OM, sulfates and nitrates) accumulation mode mass due to the presence of dust.

The left panel of Fig. 16 shows five number distributions examples. The blue and the red lines are the observations from INTEX-B for the pollution dominated aerosol and for the mixed aerosol types. The green distribution is a simulated distribution with only a 10% reduction in the pollution NMD. The magenta line is the "base case" from the sensitivity analysis by Boucher and Anderson (1995) while the black line is the "water soluble" aerosol type from the popular Optical Properties of Aerosols and Clouds (OPAC) parameterization (Hess et al., 1998). The log-normal fitting parameters used to describe these distributions are found in Table 5. Scattering, calculated at 40% and 80% relative humidity, is shown in the middle and right hand plots of Fig. 16. Table 6 compares light scattering for the blue, green and red distributions by evaluating their integrals at 10%, 80% and 95% RH. From these calculations it is clear that small reductions (10–25%) in the distributions NMD has a large influence on aerosol optical properties, reducing scattering by as much as 30–70%. This concern is particularly relevant to global climate models that use static aerosol size distributions (e.g. OPAC), or those that use modal or sectional approaches that cannot capture the dynamic nature of the aerosol number distribution.

In Fig. 16 and Table 6 we modeled the optical properties by assigning a growth factor consistent with an ammonium sulfate type composition and by varying the refractive index as a function of RH. The parameter γ, used in the f(RH) function (Eq. 1), implicitly incorporates the effects that water uptake, aerosol size, and changing refractive index have on aerosol optical properties. For the pollution distribution with an NMD 0.10 μm (blue in Fig. 16), the ammonium sulfate type composition results in a γ value of ~0.76. Strictly speaking it is not appropriate to apply this γ to the other two distributions (NMD=0.090 μm and 0.075 μm) as their γ values are uniquely dependent on

their size distributions and composition. However, Fig. 17 plots the explicitly calculated scattering values as a function of RH compared to those generated using a static γ of 0.76 for each distribution. Table 7 tabulates the difference between the static γ values compared to the explicitly calculated scattering values at 10%, 80% and 95% RH. As indicated, the static γ method tends to over predict scattering by ~10–25% at relative humidities below 95%. The static γ method does however have an advantage. Since actual aerosol composition, their diameter growth factors – g(RH), and refractive indices are poorly constrained, we can use the static γ approximation to evaluate the effects of size versus composition on aerosol optical properties for these examples.

The INTEX-B, free troposphere, total aerosol, average f(RH) γ is 0.49–0.52 (Table 4). This value is effectively identical to the ACE-Asia average 0.51 for fine mode dominated total aerosol (Anderson et al., 2003), indistinguishable from pollution dominated FT values over North America (0.47±0.7) (CM^c, unpublished data, INTEX-NA), but lower than the ACE-Asia value, 0.63, in the pollution dominated MBL (Carrico et al., 2003). The ACE-Asia version of the Quinn et al. (2005) parameterization of f(RH) γ,

$$\gamma_s = 0.9 - 0.7F_o \tag{3}$$

allows us to estimate the ratio of particulate organic matter to POM+SO_4^{2-} according to:

$$F_o = \frac{C_o}{(C_o + C_s)} \tag{4}$$

where C_o is the mass of POM and C_s is the mass of sulfates. POM can be further divided into both semivolatile (SVolOM) and refractory (RefOM) organic components (Clarke et al., 2007). For an f(RH) γ of 0.50, F_o is 0.57. As discussed in Sect. 4.1 the INTEX-B average refractory volume fraction is ~12–16%, ±7%. Assigning a density of 1.3 g cm^{-3} to both the refractory and semivolatile OM mass material (Cross et al., 2007) we can break the C_o=0.57 term into C_o=0.09+0.48 (RefOM+SVolOM mass). We can now evaluate the effect a 25% or 50% reduction in volatile accumulation mode mass (SVolOM+sulfates) has on F_o in order to predict the attendant reduction in f(RH)

γ. The corresponding for values for F_o are 0.58 and 0.60 and result in new f(RH) γ values of 0.49 and 0.48. Table 8 briefly summarizes the comparison between reductions in light scattering due to aerosol size compared to changes in composition. A 10–25% reduction in the size distribution NMD leads to a 30–70% reduction in light scattering. After reducing the accumulation mode semi-volatile inorganic (i.e. sulfates) and organic mass by 50%, light scattering at 80% RH only decreases by ~3%. Thus we conclude that reductions in ambient light scattering, due to competition between pollution and dust aerosol surface area for condensing secondary species, is dominated by reductions in median aerosol size, and not changes to accumulation mode aerosol hygroscopicity.

4.3 The effect of heterogenous reactions on NO_y

In Sect. 4.0 we established that the heterogeneous reactions are occurring between gas-phase nitrogen species (e.g. HNO_3, NO_2) and mineral dust during long-range transport from Asia. These reactions result in the sequestering of gas-phase compounds in the supermicrometer particulate phase. These relations are replotted in Fig. 18 to examine the effect of Asian dust on NO_y. Here NO_y is defined as the sum of the in-situ measurements of NO, NO_2, HNO_3, PNs and ANs. The left panel shows that nitric acid is converted into aerosol nitrate and is reduced to ~20% of the sum of these two species at high dust concentrations. Pollution dominated airmasses are rich in NO_y but particulate NO_3^- is <~20% of the total nitrogen species (top-center and right of Fig. 18). As dust mass increases, particulate nitrate is created from NO_y and becomes a larger fraction (20-40%) of total nitrogen. Recall that these estimates are somewhat conservative as the DC-8 measurements of gas-phase HNO_3 are likely contaminated with aerosol NO_3^- (Miyazaki et al., 2005; Zondlo et al., 2003).

Whereas the filter-based measurements of aerosol chemistry are slow (300–600 s), the HiGEAR size distribution measurements are relatively fast (3 s). In Fig. 5 we established a robust (R^2=0.90) regression of 11 wt% for the $CaCO_3$ present in the Asian dust samples. In Figs. 7, 9, 11 and 14 we show that 10–25% of the $CaCO_3$ has been

consumed by reacting to form $Ca(NO_3)_2$. Assuming an 11 wt% for the dust calcite content and 25% consumption of this alkalinity, we explore the ratios of aerosol nitrate to HNO_3 and NO_y using 60-s averages of HNO_3, NO_y and supermicrometer dust. Data are restricted to the Pacific FT (alt>2.0 km, O_3<200 ppbv), west of 125° W where fast submicrometer sulfate concentrations are above 1.0 $\mu g\,sm^{-3}$. The results of this simulation are shown in the bottom panels of Fig. 18 using red circles. In general we have replicated the shape of the measured relation. The main discrepancy is that the simulated ratios have values higher than those observed using the slower chemistry measurements. This can be attributed to the fact that the tail of the dust distribution has been shown to extend below the 1 μm cut size used to isolate the supermicrometer dust and nitrate mass (see also Clarke et al., 2004) and the use of 25% conversion of the $CaCO_3$, an upper bound. In addition, some nitrate is present as submicrometer NH_4NO_3 and has not been accounted for.

We can also examine these relationships using the fast chemistry measurements from the NSF/NCAR C-130 data collected off the US west coast during INTEX-B. The nitrogen ratios are shown in the upper three panels of Fig. 19 for measurements aboard the C-130. These data are stratified using the same criteria as Dunlea et al. (2008), but do not show the same characteristics as the INTEX-B data (e.g. reduction in NO_y:total nitrogen versus Ca^{2+} or dust). The reason for this difference is that, although fast, the HR-ToF-AMS only measures non-refractory NO_3^- in the submicrometer mode, whereas most (~>70%) of the nitrate is dust-bound in the supermicrometer mode (Kline et al., 2004). Still, the far right panel of Fig. 19 shows an interesting trend in the AMS measurements of NO_3^-. There is a slight reduction of NO_y:total nitrogen as a function of dust mass. This could be attributed to $Ca(NO_3)_2$ detected by the HR-ToF-AMS below 1.0 μm, in the lower-tail of the dust distribution. As in Fig. 18, we can estimate coarse-mode nitrate using the fast size distribution measurements aboard the C-130 data. This is shown in the bottom three panels of Fig. 19 and is an approximation to the chemistry-based measurements presented in the top row of Fig. 8.

The upper panel from Fig. 18 and the lower panel from Fig. 19 give us the most com-

plete picture of the heterogeneous reactions we have observed. The observations support the findings of Song and Carmichael (2001), who predicted that in the presence of dust "more than 50% of the HNO_3 has partitioned onto dust particles". Second, the presence of dust irreversibly sequesters NO_y species in the particulate phase. Without dust (<5 $\mu g\,sm^{-3}$) NO_y accounts for ~>85% of the total nitrogen. When dust concentrations exceed ~10 $\mu g\,sm^{-3}$, coarse nitrate formation reduces the NO_y fraction such that it accounts for 60–80% of total nitrogen. This is in good agreement with Phadnis and Carmichael (2000) who predicted that "the presence of dust [increases] particle nitrate levels in East Asia by ~40%".

5 Conclusions

In spring 2006 the NASA DC-8 and the NSF/NCAR C-130 measured trace-gases and aerosol over Mexico and the Eastern North Pacific as part of MILAGRO and INTEX-B. Airmasses transported long-range from East Asia were sampled in the free troposphere and found to contain Asian pollution and Asian pollution mixed with dust. Accumulation mode and supermicrometer size distributions are summarized and fit using log-normal functions. The presence of dust is found to reduce the median diameter of the accumulation mode aerosol by up to 25% due to competition for condensing secondary aerosol species. Adding secondary aerosol mass to the supermicrometer mode through condensation and/or heterogeneous reactions has a negligible effect on dust hygroscopicity and optical properties. However, altering the median diameter of the accumulation mode aerosol by 10–25% can reduce light scattering values by factors of 30–70%. Accounting for the relative enrichment of hydrophobic species in dust-influenced accumulation mode aerosol results in a further reduction in light scattering of ~3% at 80% relative humidity. Thus we conclude that the reduction in accumulation mode aerosol size, and not subtle changes to its composition, dominates the effect of mineral dust on accumulation mode aerosol optical properties. In order to better predict

the influence of heterogeneous reactions on aerosol direct and indirect effects, climate modelers are encouraged to improve the dynamic representation of the aerosol size distribution and include source dependent chemical composition.

Recent modeling studies have been found to make incorrect assumptions regarding the solubility of Asian dust. Literature review, and in-situ measurements presented here, supports a $CaCO_3$ wt% of between 3.6 and 21% with an average value near 12% for natural Asian dust aerosol. The remaining mineral dust is composed of aluminosilicates and metal-oxides whose water uptake and activation in cloud is a strong function of size, aggregate composition, and exposure to reactive sulfur and nitrogen compounds (Grassian, 2001; Kelly et al., 2007; Matsuki et al., 2009). TRACE-P (Jordan et al., 2003a), ACE-Asia (Kline et al., 2004), MILAGRO and INTEX-B results, as well as long-term measurements at Mauna Loa Observatory show that only 10–30% of the $CaCO_3$ present in Asian dust is consumed to form more soluble $CaSO_4$ or $Ca(NO_3)_2$. As a result, only 1.2–3.6% of the dust mass could be considered "soluble" due to heterogeneous reactions.

Reacting NO_2 and/or HNO_3 with $CaCO_3$ results in an irreversible sequestering of gas-phase nitrogen species into the particulate phase. In the presence of dust, nitric acid concentrations are reduced to <50% of total nitrate (nitric acid plus particulate nitrate). NO_y as a fraction of total nitrogen (NO_y plus particulate nitrate), is reduced from >85% to 60–80% in the presence of dust. These observations may have a number of implications for atmospheric oxidants which deserve further study.

Acknowledgements. We gratefully acknowledge M. Avery for providing DC-8 measurements of O_3. We appreciate the use of Barry Huebert's MLO data, which was collected under NSF grants ATM01-04532 and ATM04-41274. This research was funded under NASA Grant: NNG06GA90G and NSF Grant: ATM05-11521. ED, PFD, and JLJ were supported by NASA grant NNG06GB03G and NSF grant ATM-0513116. This is SOEST publication number 7622.

References

Aiken, A. C., Salcedo, D., Cubison, M. J., Huffman, J. A., DeCarlo, P. F., Ulbrich, I. M., Docherty, K. S., Sueper, D., Kimmel, J. R., Worsnop, D. R., Trimborn, A., Northway, M., Stone, E. A., Schauer, J. J., Volkamer, R., Fortner, E., de Foy, B., Wang, J., Laskin, A., Shutthanandan, V., Zheng, J., Zhang, R., Gaffney, J., Marley, N. A., Paredes-Miranda, G., Arnott, W. P., Molina, L. T., Sosa, G., and Jimenez, J. L.: Mexico City aerosol analysis during MILAGRO using high resolution aerosol mass spectrometry at the urban supersite (T0) – Part 1: Fine particle composition and organic source apportionment, Atmos. Chem. Phys. Discuss., 9, 8377–8427, 2009, http://www.atmos-chem-phys-discuss.net/9/8377/2009/.

Alfaro, S. C., Gomes, L., Rajot, J. L., Lafon, S., Gaudichet, A., Chatenet, B., Maille, M., Cautenet, G., Lasserre, F., Cachier, H., and Zhang, X. Y.: Chemcial and optical characterizatino of aerosols measured in spring 2002 at the ACE-ASia supersite, Zhenbeitai, China, J. Geophys. Res., 108(D23), 8641, doi:10.1029/2002JD003214, 2003.

Anderson, T. L., Covert, D. S., Marshall, S. F., Laucks, M. L., Charlson, R. J., Waggoner, A. P., Ogren, J. A., Caldow, R., Holm, R. L., Quant, F. R., Sem, G. J., Wiedensohler, A., Ahlquist, N. A., and Bates, T. S.: Performance characteristics of a high-sensitivity, three-wavelength, total scatter/backscatter nephelometer, J. Atmos. Oceanic Technol., 13(5), 967–986, 1996.

Anderson, T. L., Masonis, S. J., Covert, D. S., Ahlquist, N. C., Howell, S. G., Clarke, A. D., and McNaughton, C. S.: Variability of aerosol optical properties derived from in situ aircraft measurements during ACE-Asia, J. Geophys. Res., 108(D23), ACE 15-1–ACE 15-19, 2003.

Anderson, T. L. and Ogren, J. A.: Determining aerosol radiative properties using a TSI 3563 integrating nephelometer, Aerosol Sci. Technol., 29, 57–69, 1998.

Andreae, M. O. and Crutzen, P. J.: Atmospheric Aerosols: Biogeochemical Sources and Role in Atmospheric Chemistry, Science, 276(5315), 1052–1058, 1997.

Archuleta, C. M., DeMott, P. J., and Kreidenweis, S. M.: Ice nucleation by surrogates for atmospheric mineral dust and mineral dust/sulfate particles at cirrus temperatures, Atmos. Chem. Phys., 5, 2617–2634, 2005, http://www.atmos-chem-phys.net/5/2617/2005/.

Arimoto, R., Zhang, X. Y., Huebert, B. J., Kang, C. H., Savoie, D. L., Prospero, J. M., Sage, S. K., Schloesslin, C. A., Khaing, H. M., and Oh, S. N.: Chemical composition of atmospheric aerosols from Zhenbeitai, China and Gosan, South Korea, during ACE-Asia, J. Geophys. Res., 109, D19S04, doi:10.1029/2003JD004323, 2004.

Baron, P. A. and Willeke, K.: Aerosol Measurement: Principles, techniques, and applications,

Second edition, John Wiley and Sons, Inc., 2001.
Bauer, S. E. and Koch, D.: Impact of heterogeneoussulfate formation at mineral dust surfaces on aerosol loads and radiative forcing in the Goddard Institute for Space Studies general circulation model, J. Geophys. Res., 110, D17202, doi:10.1029/2005JD005870, 2005.
Bauer, S. E., Mishchenko, M. I., Lacis, A. A., Zhang, S., Perlwitz, J., and Metzger, A. M.: Do sulfate and nitrate coatings on minearl dust have important effects on radiative properties and climate modelling?, J. Geophys. Res., 112, D06307, doi:10.1029/2005JD006977, 2007.
Bergin, M. H., Ogren, J. A., Schwartz, S. E., and McInnes, L. M.: Evaporation of ammonium nitrate aerosol in a heated nephelometer: Implications for field measurements, Environ. Sci. Technol., 31(10), 2878–2883, 1997.
Blomquist, B. W., Huebert, B. J., Howell, S. G., Litchy, M. R., Twohy, C. H., Schanot, A., Baumgardner, D., Lafleur, B., Seebauch, R., and Laucks, M. L.: An evaluation of the community aerosol inlet for the NCAR C-130 research aircraft, J. Atmos. Oceanic Technol., 18(8), 1387–1397, 2001.
Bond, T. C., Bussemer, M., Wehner, B., Keller, S., Charlson, R. J., and Heintzenberg, J.: Light absorption by primary particle emissions from a lignite burning plant, Environ. Sci. Technol., 33(21), 3887–3891, 1999.
Boucher, O. and Anderson, T. L.: General circulation model assessment of the sensitivity of direct climate forcing by anthropogenic sulfate aerosols to aerosol size and chemistry, J. Geophys. Res., 100(D12), 26117–26134, 1995.
Brock, C. A., Sullivan, A. P., Peltier, R. E., Weber, R. J., Wollny, A. G., Gouw, J. A. D., Middlebrook, A. M., Atlas, E. L., Stohl, A., Trainer, M. K., Cooper, O. R., Fehsenfeld, F. C., Frost, G. J., Holloway, J. S., Hubler, G., Neuman, J. A., Ryerson, T. B., Warneke, C., and Wilson, J. C.: Sources of particulate matter in the northeastern United States in summer: 2. Evolution of chemical and microphysical properties, J. Geophys. Res., 113, D08302, doi:10.1029/2007JD009241, 2008.
Canagaratna, M. R., Jayne, J. T., Jimenez, J. L., Allan, J. D., Alfarra, M. R., Zhang, Q., Onasch, T. B., Drewnick, F., Coe, H., Middlebrook, A., Delia, A. E., Williams, L. R., Trimborn, A., Northway, M. J., DeCarlo, P. F., Kolb, C. E., Davidovits, P., and Worsnop, D. R.: Chemical and Microphysical Characterization of Ambient Aerosols with the Aerodyne Aerosol Mass Spectrometer, Mass Spectrom. Rev., 26, 185–222, 2007.
Carrico, C. M., Kus, P., Rood, M. J., Quinn, P. K., and Bates, T. S.: Mixtures of pollution, dust, sea salt, and volcanic aerosol during ACE-Asia: Radiative properties as a function of relative

humidity, J. Geophys. Res., 108(D23), ACE 18-1–ACE 18–18, 2003.
Charlson, R. J., Schwartz, S. E., Hales, J. M., Cess, R. D., Coakley, J. A., Hansen, J. E., and Hofmann, D. J.: Climate Forcing by Anthropogenic Aerosols, Science, 255(5043), 423–430, 1992.
Chen, F. H., Shi, Q., and Wang, J. M.: Environmental changes documented by sedimentation of Lake Yiema in arid China since Late Glaciation, J. Paleolimnol., 22, 159–169, 1999.
Clarke, A. D.: A thermo-optic technique for in situ analysis of size-resolved aerosol physicochemistry, Atmos. Environ., 25A, 635–644, 1991.
Clarke, A. D., Collins, W. G., Rasch, P. J., Kapustin, V. N., Moore, K., Howell, S., and Fuelberg, H. E.: Dust and pollution transport on global scales: Aerosol measurements and model predictions, J. Geophys. Res., 106(D23), 32555–32570, 2001.
Clarke, A. D., McNaughton, C., Kapustin, V. N., Shinozuka, Y., Howell, S., Dibb, J., Zhou, J., Anderson, B., Brekhovskikh, V., Turner, H., and Pinkerton, M.: Biomass burning and pollution aerosol over North America: Organic components and their influence on spectral optical properties and humidification response, J. Geophys. Res., 112, D12S18, doi:10.1029/2006JD007777, 2007.
Clarke, A. D., Shinozuka, Y., Kapustin, V. N., Howell, S., Huebert, B., Doherty, S., Anderson, T., Covert, D., Anderson, J., Hua, X., Moore, I. K. G., McNaughton, C., Carmichael, G., and Weber, R.: Size distributions and mixtures of dust and black carbon aerosol in Asian outflow: Physiochemistry and optical properties, J. Geophys. Res., 109(D15), 1–20, 2004.
Clarke, A. D., Uehara, T., and Porter, J. N.: Atmospheric nuclei and related aerosol fields over the Atlantic: Clean subsiding air and continental pollution during ASTEX, J. Geophys. Res.-Atmos., 102(D21), 25281–25292, 1997.
Clarke, A. D., Varner, J. L., Eisele, F., Mauldin, R. L., Tanner, D., and Litchy, M.: Particle production in the remote marine atmosphere: Cloud outflow and subsidence during ACE 1, J. Geophys. Res.-Atmos., 103(D13), 16397–16409, 1998.
Cohen, D. D., Garton, D., Stelcer, E., Hawas, O., Want, T., Poon, S., Kim, J., Choi, B. C., Oh, S. N., Sin, H.-J., Ko, M. Y., and Uematsu, M.: Multielemental analysis and characterization of fine aerosols at several key ACE-Asia sites, J. Geophys. Res., 109, D19S12, doi:10.1029/2003JD003569, 2004.
Craig., R. F.: Soil Mechanics, E & FN Spon, New York, 1997.
Cross, E. S., Slowik, J. G., Davidovits, P., Allan, J. D., Worsnop, D. R., Jayne, J. T., Lewis, D. K., Canagaratna, M. R., and Onasch, T. B.: Laboratory and ambient Particle Density Determi-

nations using Light Scattering in Conjunction with Aerosol Mass Spectrometry, Aerosol Sci. Technol., 4, 343–359, 2007.
Crounse, J. D., McKinney, K. A., Kwan, A. J., and Wennberg, P. O.: Measurement of gas-phase hydroperoxides by chemical ionization mass spectrometry (CIMS), Analyt. Chem., 78, 6726–6732, 2006.
Dai, A., Fung, I., and Genio, A. D. D.: Surface observed global land precipitiation variations during 1900–1988, J. Climate, 10, 2943–2962, 1997.
Davis, D. D., Chen, G., Crawford, J. H., Liu, S., Tan, D., Sandholm, S. T., Jing, P., Cunnold, D. M., DiNunno, B., Browell, E. V., Grant, W. B., Fenn, M. A., Anderson, B. E., Barrick, J. D., Sachse, G. W., Vay, S. A., Hudgins, C. H., Avery, M. A., Lefer, B., Shetter, R. E., Heikes, B. G., Blake, D. R., Blake, N., Kondo, Y., and Oltmans, S.: An assessment of western North Pacific ozone photochemistry based on springtime observations from NASA's PEM‐West B (1994) and TRACE‐P (2001) field studies, J. Geophys. Res., 108(D21), GTE 50-1–GTE 50-18, 2003.
Day, D. A., Wooldridge, P. J., Dillon, M. B., Thornton, J. A., and Cohen, R. C.: A thermal dissociation laser-induced fluorescence instrument for in-situ detection of NO_2, peroxy nitrates, alkyl nitrates, and HNO_3, J. Geophys. Res., 107(D6), 4046, doi:10.1029/2001JD000779, 2002.
DeCarlo, P. F., Dunlea, E. J., Kimmel, J. R., Aiken, A. C., Sueper, D., Crounse, J., Wennberg, P. O., Emmons, L., Shinozuka, Y., Clarke, A., Zhou, J., Tomlinson, J., Collins, D. R., Knapp, D., Weinheimer, A. J., Montzka, D. D., Campos, T., and Jimenez, J. L.: Fast airborne aerosol size and chemistry measurements above Mexico City and Central Mexico during the MILAGRO campaign, Atmos. Chem. Phys., 8, 4027–4048, 2008, http://www.atmos-chem-phys.net/8/4027/2008/.
DeCarlo, P. F., Kimmel, R. E., Trimborn, A., Northway, M. J., Jayne, J. T., Aiken, A. C., Gonin, M., Fuhrer, K., Horvath, T., Docherty, K. S., Worsnop, D. R., and Jimenez, J. L.: Field-Deployable, High-Resolution, Time-of-Flight Aerosol Mass Spectrometer, Analyt. Chem., 78, 8281–8289, 2006.
DeCarlo, P. F., Slowik, J. G., Worsnop, D. R., Davidovits, P., and Jimenez, J. L.: Particle Morphology and Density Characterization by Combined Mobility and Aerodynamic Diameter Measurements. Part 1: Theory, Aerosol Sci. Technol., 38, 1185–1205, 2004.
Dentener, F., Carmichael, G. R., Zhang, Y., Lelieveld, J., and Crutzen, P. J.: Role of mineral aerosol as a reactive surface in the global troposphere, J. Geophys. Res., 101(D17), 22869–22889, 1996.

Dentener, F., Kinne, S., Bond, T., Boucher, O., Cofala, J., Generoso, S., Ginoux, P., Gong, S., Hoelzemann, J. J., Ito, A., Marelli, L., Penner, J. E., Putaud, J.-P., Textor, C., Schulz, M., van der Werf, G. R., and Wilson, J.: Emissions of primary aerosol and precursor gases in the years 2000 and 1750 prescribed data-sets for AeroCom, Atmos. Chem. Phys., 6, 4321–4344, 2006, http://www.atmos-chem-phys.net/6/4321/2006/.

Derbyshire, E.: On the morphology, sediments, and origin of the Loess Plateau of centratl China, in: Mega-geomorphology, edited by: Gardner, R., and Scoging, pp. 172–194, Clarendon Press, Oxford, 1983.

Dibb, J. E., Talbot, R. W., Lefer, B. L., Scheuer, E., Gregory, G. L., Browell, E. V., Bradshaw, J. D., Sandholm, S. T., and Singh, H. B.: Distributions of beryllium-7 and lead-210 over the wesern Pacific: PEM West B, J. Geophys. Res., 102, 28287–28302, 1997.

Dibb, J. E., Talbot, R. W., Scheuer, E., Seid, G., DeBell, L., Lefer, B., and Ridley, B.: Stratospheric influence on the northern North American free troposphere during TOPSE: 7 Be as a stratospheric tracer, J. Geophys. Res., 108(D4), TOP 11-1–TOP 11-8, 2003a.

Dibb, J. E., Talbot, R. W., Scheuer, E. M., Seid, G., Avery, M. A., and Singh, H. B.: Aerosol chemical composition in Asian continental outflow during the TRACE-P campaign: Comparison with PEM-West B, J. Geophys. Res., 108(D21), GTE 36-1–GTE 36-13, 2003b.

Ding, Z. L., Sun, J. M., Yang, S. L., and Liu, T. S.: Geochemistry of the Pliocene red clay formation in the Chinese Loess Plateau and implications for its origin, source provenance and palioclimate change, Geochimica Et Cosmochimica Acta, 65(6), 901–913, 2001.

Dunlea, E. J., DeCarlo, P. F., Aiken, A. C., Kimmel, J. R., Peltier, R. E., Weber, R. J., Tomlison, J., Collins, D. R., Shinozuka, Y., McNaughton, C. S., Howell, S. G., Clarke, A. D., Emmons, L. K., Apel, E. C., Pfister, G. G., van Donkelaar, A., Martin, R. V., Millet, D. B., Heald, C. L., and Jimenez, J. L.: Evolution of Asian aerosols during transpacific transport in INTEX-B, Atmos. Chem. Phys. Discuss., 8, 15375–15461, 2008, http://www.atmos-chem-phys-discuss.net/8/15375/2008/.

Eastwood, M. L., Cremel, S., Wheeler, M., Murray, B. J., Girard, E., and Bertram, A. K.: Effects of sulfuric acid and ammonium sulfate coatings on the ice nucleation properties of kaolinite particles, Geophys. Res. Lett., 36, L02811, doi:10.1029/2008GL035997, 2009.

Fan, S.-M., Horowitz, L. W., Levy II, H., and Moxim, W. J.: Impact of air pollution on wet deposition of mineral dust aerosols, Geophys. Res. Lett., 31, L02104, doi:10.1029/2003GL018501, 2004.

Fast, J. D., de Foy, B., Acevedo Rosas, F., Caetano, E., Carmichael, G., Emmons, L., McKenna,

D., Mena, M., Skamarock, W., Tie, X., Coulter, R. L., Barnard, J. C., Wiedinmyer, C., and Madronich, S.: A meteorological overview of the MILAGRO field campaigns, Atmos. Chem. Phys., 7, 2233–2257, 2007, http://www.atmos-chem-phys.net/7/2233/2007/.

Fuller, K. A., Malm, W. C., and Kreidenweis, S. M.: Effects of mixing on extinction by carbonaceous particles, J. Geophys. Res., 104(D13), 15941–15954, 1999.

Ginoux, P., Chin, M., Tegen, I., Prospero, J. M., Holben, B., Dubovik, O., and Lin, S.: Sources and distributions of dust aerosol simulated with the GOCART model, J. Geophys. Res., 106(D17), 20255–20273, 2001.

Grassian, V. H.: Heterogeneous uptake and reaction of nitrogen oxides and volatile organic compounds on the surface of atmospheric particles including oxides, carbonates, soot and mineral dust: Implications for the chemical balance of the troposphere, Int. Rev. Phys. Chem., 20(3), 467–548, 2001.

Hand, J. L. and Kreidenweis, S. M.: A new method for retrieving particle refractive index and effective density from aerosol size distribution data, Aerosol Sci. Technol., 36, 1012–1026, 2002.

Harvey, M.: The iron CLAW, Environ. Chem., 4, 396–399, 2007.

Hess, M., Koepke, P., and Schult, I.: Optical properties of aerosols and clouds: The software package OPAC, B. Am. Meteor. Soc., 79(5), 831–844, 1998.

Howell, S. G., Clarke, A. D., Shinozuka, Y., Kapustin, V. N., McNaughton, C. S., Huebert, B. J., Doherty, S., and Anderson, T.: The Influence of relative humidity upon pollution and dust during ACE-Asia: size distributions and implications for optical properties, J. Geophys. Res., 111, D06205, doi:10.1029/2004JD005759, 2006.

Huebert, B. J., Howell, S. G., Covert, D. S., Bertram, T., Clarke, A. D., Anderson, J. R., Lafleur, B., Seebaugh, W. R., Wilson, J. C., Gesler, D., Blomquist, B. W., and Fox, J.: PELTI: Measuring the passing efficiency of an airborne low turbulence aerosol inlet, Aerosol Sci. Technol., 38, 803–826, doi:10.1080/027868290500823, 2004.

Huebert, B. J., Phillips, C. A., Zhuang, L., Kjellstrom, E., Rodhe, H., Feichter, J., and Land, C.: Long-term measurements of free-tropospheric sulfate at Mauna Loa: Comparison with global model simulations, J. Geophys. Res.-Atmos., 106(D6), 5479–5492, 2001.

Huffman, J. A., Ziemann, P. J., Jayne, J. T., Worsnop, D. R., and Jimenez, J. L.: Development and Characterization of a Fast-Stepping/Scanning Thermodenuder for Chemically-Resolved Aerosol Volatility Measurements, Aerosol Sci. Technol., 42, 395–407, 2008.

Husar, R. B., Tratt, D. M., Schichtel, B. A., Falke, S. R., Li, F., Jaffe, D., Gasso, S., Gill, T.,

Laulainen, N. S., Lu, F., Reheis, M. C., Chun, Y., Westphal, D. L., Holben, B. N., Gueymard, C., McKendry, I., Kuring, N., Feldman, G. C., McClain, C. R., Frouin, R., Merrill, C., Dubois, M., Vignola, F., Murayama, T., Nickovic, S., Wilson, W. E., Sassen, K., Sugimoto, N., and Malm, W. C.: Asian dust events of April 1998, J. Geophys. Res., 106(D16), 18317–18330, 2001.

Jacob, D. J.: Heterogeneous chemistry and tropospheric ozone, Atmos. Environ., 34, 2131–2159, 2000.

Jordan, C. E., Dibb, J. E., Anderson, B. E., and Fuelberg, H. E.: Uptake of nitrate and sulfate on dust aerosols during TRACE-P, J. Geophys. Res., 108(D21), GTE 38-1–GTE 38-10, 2003a.

Jordan, C. E., Dibb, J. E., and Finkel, R. C.: ^{10}Be/^{7}Be tracer of atmospheric transport and stratosphere-troposphere exchange, J. Geophys. Res., 108(D8), ACL 3-1–ACL 3–14, 2003b.

Karl, D. M. and Lukas, R. B.: The Hawaii Ocean Time-series (HOT) program: Background, rationale and field implementation, Deep-Sea Res. II, 43, 129–156, 1996.

Kelly, J. T., Chuang, C. C., and Wexler, A. S.: Influence of dust composition on cloud droplet formation, Atmos. Environ., 41, 2904–2916, 2007.

Kim, S., Huey, L. G., Stickel, R. E., Tanner, D. J., Crawford, J. H., Olson, J. R., Chen, G., Brune, W. H., Ren, X., Lesher, R., Wooldridge, P. J., Bertram, T. H., Perring, A. E., Cohen, R. C., Lefer, B., Shetter, R. E., Avery, M., Diskin, G., and Sokolik, I.: Measurement of pernitric acid in the free troposphere, J. Geophys. Res., 112, D12S01, doi:10.1029/2006JD007676, 2007.

Kinne, S., Schulz, M., Textor, C., et al.: An AeroCom initial assessment – optical properties in aerosol component modules of global models, Atmos. Chem. Phys., 6, 1815–1834, 2006, http://www.atmos-chem-phys.net/6/1815/2006/.

Kline, J., Huebert, B., Howell, S., Blomquist, B., Zhuang, J., Bertram, T., and Carrillo, J.: Aerosol composition and size versus altitude measured from the C-130 during ACE-Asia, J. Geophys. Res., 109(D19), 1–22, 2004.

Lafon, S., Sokolik, I., Rajot, J., Caquineau, S., and Gaudichet, A.: Characterization of iron oxides in mineral dust aerosols: Implications for light absorption, J. Geophys. Res., 111, D21207, doi:10.1029/2005JD007016, 2006.

Lammel, G. and Novakov, T.: Water nucleation properties of carbon black and diesel soot particles, Atmos. Environ., 29, 813–823, 1995.

Liao, H. and Seinfeld, J. H.: Global impacts of gas-phase chemistry-aerosol interactions on direct radiative forcing by anthropogenic aerosol and ozone, J. Geophys. Res., 110, D18208,

doi:10.1029/2005JD005907, 2005.
Liu, T.: Loess in China, China Ocean Press, Beijing, 1985.
Maring, H., Savoie, D. L., Izaguirre, M. A., Custals, L., and Reid, J. S.: Mineral dust aerosol size distribution change during atmospheric transport, J. Geophys. Res., 108(D19), PRD 8-1–PRD 8-6, 2003.
Martin, J. H.: Glacial-interglacial CO_2 change: the iron hypothesis, Paleooceanography, 5(1), 1–13, 1990.
Martin, R. V., Jacob, D. J., Yantosca, R. M., Chin, M., and Ginoux, P.: Global and regional decreases in tropospheric oxidants from photochemical effects of aerosols, J. Geophys. Res., 108(D3), 4097, doi:10.1029/2002JD002622, 2003.
Matsuki, A., Schwarzenboeck, A., Venzac, H., Laj, P., Crumeyrolle, S., and Gomes, L.: Effect of surface reaction on the cloud nucleating properties of mineral dust: AMMA aircraft campaign in summer 2006, Atmos. Chem. Phys. Discuss., 9, 1797–1830, 2009, http://www.atmos-chem-phys-discuss.net/9/1797/2009/.
Mayol-Bracero, O. L., Gabriel, R., Andreae, M. O., Kirchstetter, T. W., Novakov, T., Ogren, J., Sheridan, P., and Streets, D. G.: Carbonaceous aerosols over the Indian Ocean during the Indian Ocean Experiment (INDOEX): Chemical characterization, optical properties, and probable sources, J. Geophys. Res., 107(D19), INX2 29-1–INX2 29-21, 2002.
McNaughton, C. S., Clarke, A. D., Howell, S. G., Pinkerton, M., Anderson, B., Thornhill, L., Hudgins, C., Winstead, E., Dibb, J. E., Scheuer, E., and Maring, H.: Results from the DC-8 Inlet Characterization Experiment (DICE): Airborne versus surface sampling of mineral dust and sea salt aerosols, Aerosol Sci. Technol., 41(2), 136–159, 2007.
Miyazaki, Y., Kondo, Y., Takegawa, N., Weber, R. J., Koike, M., Kita, K., Fukuda, M., Ma, Y., Clarke, A. D., Kapustin, V. N., Flocke, F., Weinheimer, A. J., Zondlo, M., Eisele, F. L., Blake, D. R., and Liley, B.: Contribution of particulate nitrate to airborne measurements of total reactive nitrogen, J. Geophys. Res., 110, D15304, doi:10.1029/2004JD005502, 2005.
Molina, L. T., Kolb, C. E., de Foy, B., Lamb, B. K., Brune, W. H., Jimenez, J. L., Ramos-Villegas, R., Sarmiento, J., Paramo-Figueroa, V. H., Cardenas, B., Gutierrez-Avedoy, V., and Molina, M. J.: Air quality in North America's most populous city – overview of the MCMA-2003 campaign, Atmos. Chem. Phys., 7, 2447–2473, 2007, http://www.atmos-chem-phys.net/7/2447/2007/.
Moulin, C. and Chiapello, I.: Impact of human-induced desertification on the intensification of Sahel dust emission and export over the last decades, Geophys. Res. Lett., 33, L18808,

doi:10.1029/2006GL025923, 2006.
Nicholson, S. E., Tucker, C. J., and Ba, M. B.: Desertification, drought, and surface vegetation: An example from the West African Sahel, B. Am. Meteor. Soc., 79(5), 815–829, 1998.
Osborne, S. R. and Haywood, J. M.: Aircraft observations of the microphysical and optical properties of major aerosol species, Atmos. Res., 73, 173–201, 2005.
Penner, J. E., Quaas, J., Storelvmo, T., Takemura, T., Boucher, O., Guo, H., Kirkevåg, A., Kristjánsson, J. E., and Seland, Ø.: Model intercomparison of indirect aerosol effects, Atmos. Chem. Phys., 6, 3391–3405, 2006, http://www.atmos-chem-phys.net/6/3391/2006/.
Petch, J. C.: Using a cloud-resolving model to study the effects of subgrid-scale variations in relative humidity on direct sulphate-aerosol forcing, Q. J. Roy. Meteor. Soc., 127(577), 2385–2394, 2001.
Phadnis, M. J. and Carmichael, G. R.: Numerical investigation of the influence of mineral dust on the tropospheric chemistry of East Asia, J. Atmos. Chem., 36(3), 285–323, 2000.
Porter, J. N. and Clarke, A. D.: Aerosol size distribution models based on in situ measurements, J. Geophys. Res.-Atmos., 102(D5), 6035–6045, 1997.
Prospero, J. M.: Long-range transport of mineral dust in the global atmosphere: Impact of African dust on the environment of the southeastern United States, Proceedings of the National Academy of Sciences of the United States of America, 96, 3396–3403, 1999.
Qizhong, W., Haizhi, Z., and Jinluan, G.: Some geochemical problems of the loess in the middle reaches of the Huanghe (Yellow) River. The problems of quaternary geology, Science Press, Beijing, 1964.
Quinn, P. K., Bates, T. S., Baynard, T., Clarke, A. D., Onasch, T., Wang, W., Rood, M. J., Andrews, E., Allan, J., Carrico, C. M., Coffmann, D., and Worsnop, D.: Impact of particulate organic matter on the relative humidity dependence of light scattering: A simplified parameterization, Geophys. Res. Lett., 32, L22809, doi:10.1029/2005GL024322, 2005.
Reid, J. S., Jonsson, H. H., Maring, H. B., Smirnov, A., Savoie, D. L., Cliff, S. S., Reid, E. A., Livingston, J. M., Meier, M. M., Dubovik, O., and Tsay, S. C.: Comparison of size and morphological measurements of coarse mode dust particles from Africa, J. Geophys. Res., 108(D19), PRD 9-1–PRD 9-28, 2003.
Rosenfeld, D., Rudich, Y., and Lahav, R.: Desert dust suppressing precipitation: A possible desertification feedback loop, Proceedings of the National Academy of Sciences of the United States of America, 98(11), 5975–5980, 2001.
Salcedo, D., Onasch, T. B., Dzepina, K., Canagaratna, M. R., Zhang, Q., Huffman, J. A., De-

Carlo, P. F., Jayne, J. T., Mortimer, P., Worsnop, D. R., Kolb, C. E., Johnson, K. S., Zuberi, B., Marr, L. C., Volkamer, R., Molina, L. T., Molina, M. J., Cardenas, B., Bernabé, R. M., Márquez, C., Gaffney, J. S., Marley, N. A., Laskin, A., Shutthanandan, V., Xie, Y., Brune, W., Lesher, R., Shirley, T., and Jimenez, J. L.: Characterization of ambient aerosols in Mexico City during the MCMA-2003 campaign with Aerosol Mass Spectrometry: results from the CENICA Supersite, Atmos. Chem. Phys., 6, 925–946, 2006, http://www.atmos-chem-phys.net/6/925/2006/.

Sassen, K.: Indirect climate forcing over the western US from Asian dust storms, Geophys. Res. Lett., 29(10), 1465, doi:10.1029/2001GL014051, 2002.

Sassen, K., DeMott, P. J., Prospero, J. M., and Poellot, M. R.: Saharan dust storms and indirect aerosol effects on clouds: CRYSTAL-FACE results, Geophys. Res. Lett., 30(12), 1633, doi:10.1029/2003GL017371, 2003.

Scheuer, E., Talbot, R. W., Dibb, J. E., Seid, G. K., DeBell, L., and Lefer, B.: Seasonal distributions of fine aerosol sulfate in the North American Arctic basin during TOPSE, J. Geophys. Res., 108(D4), TOP 18-1–TOP 18-11, 2003.

Schnaiter, M., Linke, C., Möhler, O., Naumann, K.-H., Saathoff, H., Wagner, R., Schurath, U., and Wehner, B.: Absorption amplification of black carbon internally mixed iwth secondary organic aerosol, J. Geophys. Res., 110, D19204, doi:10.1029/2005JD006046, 2005.

Seinfeld, J. H. and Pandis, S. N.: Atmospheric chemistry and physics: from air pollution to climate change, John Wiley and Sons, New York, 1998.

Sheehy, D.: A perspective on desertification of grazingland and ecosystems in North China, Ambio, 21, 303–307, 1992.

Singh, H. B., Brune, W. H., Crawford, J. H., Jacob, D. J., Russell, P. B., et al.: An overview of the INTEX-B campaign: Transport and Transformation of Pollutants over the Pacific and Gulf of Mexico, Atmos. Chem. Phys., in preparation, 2009.

Sjostedt, S., Huey, L. G., Tanner, D. J., Peischl, J., Chen, G., Dibb, J. E., Lefer, B., Hutterli, M. A., Beyersdorf, A. J., Blake, N. J., Blake, D. R., Sueper, D. T., Ryerson, T. B., Burkhar, J., and Stohl, A.: Observation of hydroxyl and the sum of peroxy radicals at Summit Greenland during summer 2003, Atmos. Environ., 41(24), 5122–5137, doi:10.1016/j.atmosenv.2006.06.065, 2007.

Slusher, D. L., Huey, L. G., Tanner, D. J., Flocke, F. M., and Roberts, J. M.: A thermal dissociation-chemical ionization mass spectrometer (TD-CIMS) technique for the simultaneous measurement of peroxyacul nitrates and dinitrogen pentoxide, J. Geophys. Res., 109,

D19315, doi:10.1029/2004JD004670, 2004.
Sokolik, I. N. and Toon, O. B.: Direct radiative forcing by anthropogenic airborne mineral aerosols, Nature, 381, 681–683, 1996.
Sokolik, I. N. and Toon, O. B.: Incorporation of mineralogical composition into models of the radiative properties of mineral aerosol from UV to IR wavelengths, J. Geophys. Res., 104(D8), 9423–9444, 1999.
Solomon, F., Chuang, P. Y., Meskhidze, N., and Chen, Y.: Acidic processing of mineral dust iron by anthropogenic compounds over the North Pacific Ocean, J. Geophys. Res., 114, D02305, doi:10.1029/2008JD010417, 2009.
Song, C. H. and Carmichael, G. R.: Gas-particle partitioning of nitric acid modulated by alkaline aerosol, J. Atmos. Chem., 40(1), 1–22, 2001.
Stroud, C. A., Nenes, A., Jimenez, J. L., DeCarlo, P. F., Huffman, J. A., Bruintjes, R., Nemitz, E., Delia, A. E., Toohey, D. W., Guenther, A. B., and Nandi, S.: Cloud Activating Properties of Aerosol Observed during CELTIC, J. Atmos. Sci., 65(2), 441–459, 2007.
Tang, I. N.: Thermodynamic and optical properties of mixed-salt aerosols of atmospheric importance, J. Geophys. Res., 102(D2), 1883–1894, 1997.
Tang, I. N. and Munkelwitz, H. R.: Water activities, densities, and refractive indices of aqueous sulfates and sodium nitrate droplets of atmospheric importance, J. Geophys. Res., 99(D9), 18801–18808, 1994.
Tang, I. N., Tridico, A. C., and Fung, K. H.: Thermodynamic and optical properties of sea salt aerosols, J. Geophys. Res., 102(D19), 23269–23276, 1997.
Tang, Y., Carmichael, G. R., Kurata, G., Uno, I., Weber, R., Song, C. H., Guttikunda, S. K., Woo, J. H., Streets, D. G., Wei, C., Clarke, A. D., Huebert, B., and Anderson, T. L.: Impacts of dust on regional tropospheric chemistry during the ACE-Asia experiment: A model study with observations, J. Geophys. Res., 109, D19S21, doi:10.1029/2003JD003806, 2004.
Tegen, I. and Fung, I.: Contribution to the atmospheric mineral aerosol load from land surface modification, J. Geophys. Res., 100(D9), 18707–18726, 1995.
Tegen, I. and Lacis, A. A.: Modeling of particle size distribution and its influence on the radiative properties of mineral dust aerosol, J. Geophys. Res., 101(D14), 19237–19244, 1996.
Tegen, I., Werner, M., Harrison, S. P., and Kohfeld, K. E.: Relative importance of climate and land use in determining present and future global soil dust emission, Geophys. Res. Lett., 31, L05105, 2004.
Textor, C., Schulz, M., Guibert, S., Kinne, S., Balkanski, Y., Bauer, S., Berntsen, T., Berglen, T.,

Boucher, O., Chin, M., Dentener, F., Diehl, T., Easter, R., Feichter, H., Fillmore, D., Ghan, S., Ginoux, P., Gong, S., Grini, A., Hendricks, J., Horowitz, L., Huang, P., Isaksen, I., Iversen, I., Kloster, S., Koch, D., Kirkevåg, A., Kristjansson, J. E., Krol, M., Lauer, A., Lamarque, J. F., Liu, X., Montanaro, V., Myhre, G., Penner, J., Pitari, G., Reddy, S., Seland, Ø., Stier, P., Takemura, T., and Tie, X.: Analysis and quantification of the diversities of aerosol life cycles within AeroCom, Atmos. Chem. Phys., 6, 1777–1813, 2006, http://www.atmos-chem-phys.net/6/1777/2006/.

Thornton, J. A., Wooldridge, P. J., and Cohen, R. C.: Atmospheric NO_2: In-situ laser-induced fluorescence detection at parts per trillion mixing ratios, Analyt. Chem., 72(3), 528–539, 2000.

Ullerstam, C. R., Vogt, R., Langer, S., and Ljungstrom, E.: The kinetics and mechanism of SO_2 oxidation by O_3 on mineral aerosol, Phys. Chem. Chem. Phys., 4, 4694–4699, 2002.

Underwood, G. M., Song, C. H., Phadnis, M., Carmichael, G. R., and Grassian, V. H.: Heterogeneous reactions of NO_2 and HNO_3 on oxides and mineral dust: A combined laboratory and modeling study, J. Geophys. Res.-Atmos., 106(D16), 18055–18066, 2001.

Usher, C. R., Al-Hosney, H., Carlos-Cuellar, S., and Grassian, V. H.: A laboratory study of the heterogeneous uptake and oxidation of sulfur dioxide on mineral dust particles, J. Geophys. Res., 107(D23), 4713, doi:10.1029/2002JD002051, 2002.

Virkkula, A., Ahlquist, N. C., Covert, D. S., Arnott, W. P., Sheridan, P. J., Quinn, P. K., and Coffman, D. J.: Modification, Calibration and a Field Test of an Instrument for Measuring Light Absorption by Particles, Aerosol Sci. Technol., 39(1), 68–83, doi:10.1080/027868290901963, 2005.

Weinheimer, A. J., Montzka, D. D., Campos, T. L., et al.: Comparison between DC-8 and ER-2 species measurements in the tropical middle troposphere, J. Geophys. Res., 103(D17), 22087–22096, 1998.

Wyslouzil, B. E., Carleton, K. L., Sonnenfroh, D. M., Rawlins, W. T., and Arnold, S.: Observations of hydration of single, modified carbon aerosols, Geophys. Res. Lett., 21, 2107–2110, 1994.

Zondlo, M. A., Mauldin, R. L., Kosciuch, E., Cantrell, C. A., and Eisele, F. L.: Development and characterization of an airborne-based instrument used to measure nitric acid during the NASA Transport and Chemical Evolution over the Pacific field experiment, J. Geophys. Res.-Atmos., 108(D20), 8793, doi:10.1029/2002JD003234, 2003.

Table 1. Laboratory comparison of PSAP instrument noise while sampling filtered air.

Unit	Owner	Experiment	Total or submicrometer sampling	Blue δ_{300} (Mm^{-1})	Green δ_{300} (Mm^{-1})	Red δ_{300} (Mm^{-1})
PSAP1	HiGEAR	INTEX-NA& MIRAGE	Total	0.56	0.56	0.56
PSAP2	LaRC	INTEX-B	Total	0.36	0.34	0.36
PSAP3	LaRC	INTEX-B	submicrometer	0.51	0.50	0.55
PSAP4	HiGEAR	MIRAGE	submicrometer			

ACPD
9, 8469–8539, 2009

Table 2. Summary of log-normal fitting results for free troposphere pollution and pollution mixed with dust airmasses sampled over the Eastern North Pacific during INTEX-B.

Region	Aerosol type	Accumulation mode				
		N (# cm^{-3})	NMD (μm)	V (μm^3 cm^{-3})	VMD (μm)	sigma_g (–)
HI	Mixed	430	0.075	0.75	0.30	1.97
	Anthro	387	0.093	0.75	0.26	1.79
AK	Mixed	433	0.074	0.73	0.30	1.98
	Anthro	423	0.11	1.3	0.27	1.70
Region	Aerosol type	Coarse mode				
		N (# cm^{-3}	NMD (μm)	V (μm^3 cm^{-3})	VMD (μm)	sigma_g (–)
HI	Mixed	5.3	0.64	7.4	3.1	2.06
	Anthro	3.5	0.56	2.6	2.5	2.03
AK	Mixed	7.9	0.50	6.8	2.8	2.13
	Anthro	1.4	0.75	1.8	2.6	1.91
Region	Aerosol type	Refractory Aitken mode				
		N (# cm^{-3})	NMD (μm)	V (μm^3 cm^{-3})	VMD (μm)	sigma_g (–)
HI	Mixed	290	0.036	0.07	0.17	2.05
	Anthro	300	0.044	0.10	0.16	1.94
AK	Mixed	300	0.044	0.06	0.12	1.79
	Anthro	350	0.053	0.17	0.18	1.88

ACPD
9, 8469–8539, 2009

Table 3. Summary of total single scatter albedo, scattering and absorption Ångstrom exponents for 300-s level leg averages during INTEX-B. "Anthro" are fine mode dominated aerosol (FMFscat>0.6) while "Mixed" aerosols are for mixtures of pollution and dust (0.3<FMFscat<0.6). The standard deviations of the means are shown in brackets.

Hawaii		*N*	Total SSA 450 nm	Total SSA 550 nm	Total SSA 700 nm	Total Ångstrom exponent Scat (450/700)	Total Ångstrom exponent Abs (470/660) Bond correction	Total Ångstrom exponent Abs (470/660) Virkkula correction
LT	Mixed	15	0.95 (0.02)	0.96 (0.02)	0.97 (0.02)	0.54 (0.22)	2.8 (1.1)	2.6 (0.9)
	Anthro	10	0.93 (0.03)	0.94 (0.03)	0.94 (0.03)	1.06 (0.34)	2.2 (0.6)	2.0 (0.6)
Alaska		N	Total SSA 450 nm	Total SSA 550 nm	Total SSA 700 nm	Total Ångstrom exponent Scat (450/700)	Total Ångstrom exponent Abs (470/660) Bond correction	Total Ångstrom exponent Abs (470/660) Virkkula correction
LT	Mixed	14	0.96 (0.02)	0.97 (0.02)	0.97 (0.02)	0.64 (0.38)	2.7 (1.5)	2.5 (1.4)
	Anthro	40	0.94 (0.01)	0.95 (0.01)	0.94 (0.02)	1.53 (0.37)	1.8 (0.4)	1.7 (0.4)
Mexico		N	Total SSA 450 nm	Total SSA 550 nm	Total SSA 700 nm	Total Ångstrom Exponent Scat (450/700)	Total Ångstrom Exponent Abs (470/660) Bond correction	Total Ångstrom Exponent Abs (470/660) Virkkula correction
LT	Anthro	52	0.94 (0.01)	0.94 (0.01)	0.94 (0.01)	1.52 (0.30)	2.2 (0.3)	2.0 (0.3)
CBL		24	0.93 (0.01)	0.93 (0.01)	0.93 (0.02)	1.50 (0.42)	2.1 (0.6)	1.9 (0.5)
MBL		56	0.96 (0.02)	0.96 (0.02)	0.96 (0.02)	1.33 (0.38)	2.0 (0.9)	1.8 (0.7)

ACPD
9, 8469–8539, 2009

Table 4. Summary of total and submicrometer f(RH) "gamma" for 300 s level leg averages during INTEX-B. "Fine" mode dominated aerosol are defined as (FMFscat>0.6) while "mixed" aerosol are for mixtures of pollution and dust where (0.3<FMFscat<0.6). The standard deviations of the means are shown in brackets.

	Hawaii	Submicrometer		Total Aerosol	
		N	gamma	*N*	gamma
LT	Mixed	9	0.39 (0.07)	2	0.34
	Anthro	7	0.44 (0.14)	2	0.52
	Alaska	**Submicrometer**		**Total Aerosol**	
		N	gamma	*N*	gamma
UT	STE – median	5	0.55 (0.15)		
LT	Mixed	8	0.32 (0.11)	4	0.29 (0.11)
	Anthro	34	0.44 (0.12)	5	0.50 (0.07)
	Mexico	**Submicrometer**		**Total Aerosol**	
		N	gamma	*N*	gamma
LT	Anthro	22	0.50 (0.07)	4	0.49 (0.01)
CBL	Anthro	9	0.39 (0.06)	3	0.32 (0.09)
MBL	Anthro	22	0.63 (0.06)	7	0.65 (0.04)

Table 5. Log-normal parameters for distributions in Fig. 16.

N (cm^{-3})	NMD (μm)	σ_g
500	0.100	1.75
500	0.900	1.75
500	0.075	1.75
500	0.070	2.00
500	0.042	2.24

Table 6. Comparison of light scattering values for size distributions with three different NMD's at 10%, 80% and 95% RH.

NMD(μm)	σ_g	Scattering (Mm^{-1}) for $(NH_4)_2SO_4$ growth factor at: 10% RH	80% RH	95% RH	Percent Difference 10% RH	80% RH	95% RH
0.100	1.75	6.3	16.1	46.5			
0.090	1.75	4.1	10.8	32.5	−35%	−33%	−30%
0.075	1.75	1.9	5.2	16.8	−70%	−67%	−64%

Table 7. Error, expressed as a percent difference, between explicit calculations of light scattering assuming an ammonium sulfate composition for three size distributions, compared to scattering values using a fixed γ, most applicable to the distribution with an NMD of 0.10 μm.

NMD(μm)	sigma_g	Scattering for (NH4)2SO4 g(RH)			Scattering for γ=0.76			Difference (%)		
		10% RH	80% RH	95% RH	10% RH	80% RH	95% RH	10% RH	80% RH	95% RH
0.100	1.75	6.3	16.1	46.5	6.3	19.7	56.6		23%	22%
0.090	1.75	4.1	10.8	32.5	4.1	12.9	36.9		19%	14%
0.075	1.75	1.9	5.2	16.8	1.9	5.9	17.0		13%	1%

Table 8. Changes to light scattering at 80% relative humidity due to a reduction in aerosol number median diameter (blue). These reductions are compared to a reduction in accumulation mode aerosol hygroscopicity from γ=0.5 to γ=0.48 (red).

NMD(μm)	sigma_g	Scat. at 10% RH	Scattering at 80% RH		Percentage Difference		
			γ=0.50	γ=0.48	Size Only	Comp. Only	Combined
0.100	1.75	6.3	13	13			−3.0%
0.090	1.75	4.1	8.7	8.4	−35%	−3.0%	−37%
0.075	1.75	1.9	4.0	3.9	−70%		−71%

ACPD
9, 8469–8539, 2009

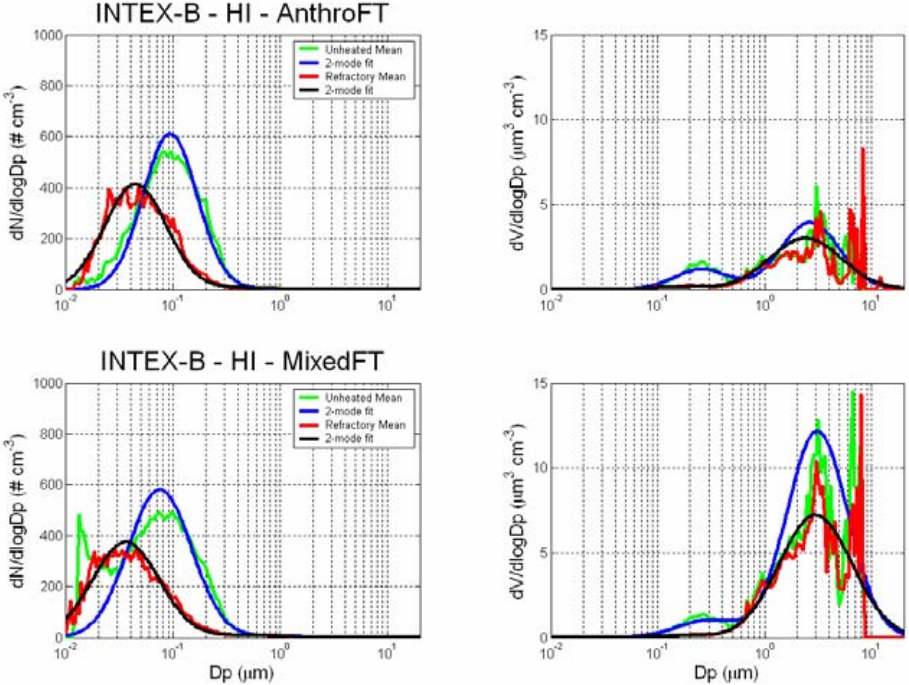

Fig. 1. Lognormal fits of the number (left) and volume (right) aerosol size distributions measured in the FT near Hawaii during INTEX-B. Total aerosol and the 2-mode fit are in green and blue while refractory aerosol is coloured red and black.

ACPD
9, 8469–8539, 2009

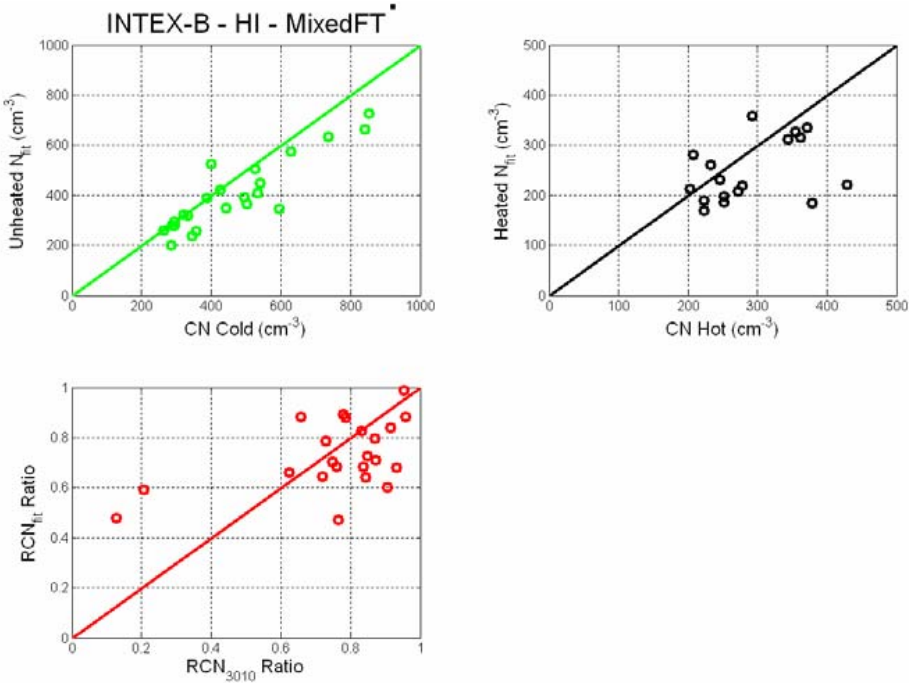

Fig. 2. Assessment of number closure between the lognormal fits to the unheated and refractory aerosol distribution and to their ratio (RCN ratio) compared to the averaged 1-Hz CN counter data.

ACPD
9, 8469–8539, 2009

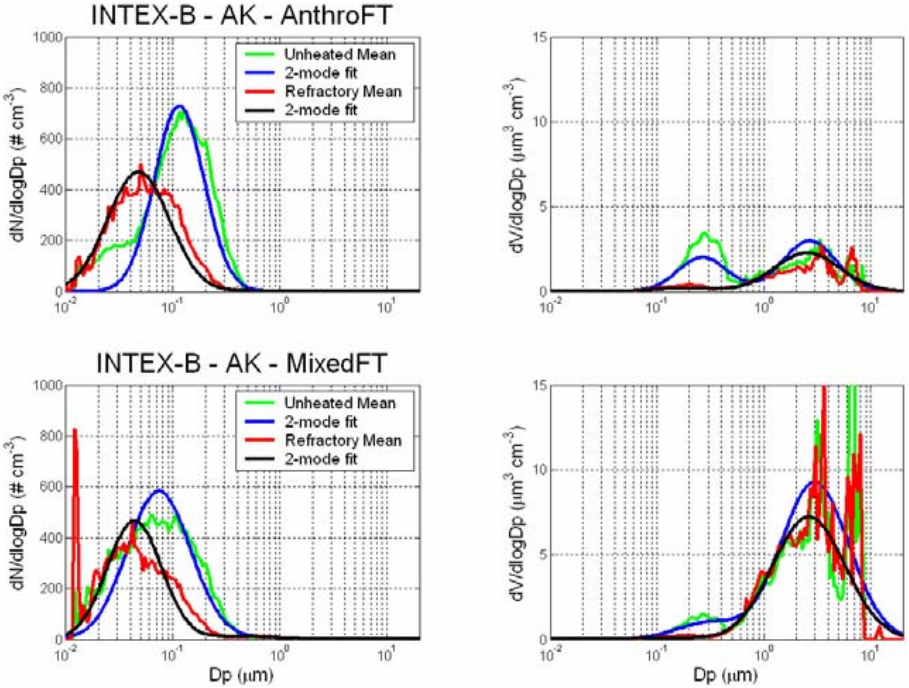

Fig. 3. Same as Fig. 1 but for data collected in the FT near Alaska.

ACPD
9, 8469–8539, 2009

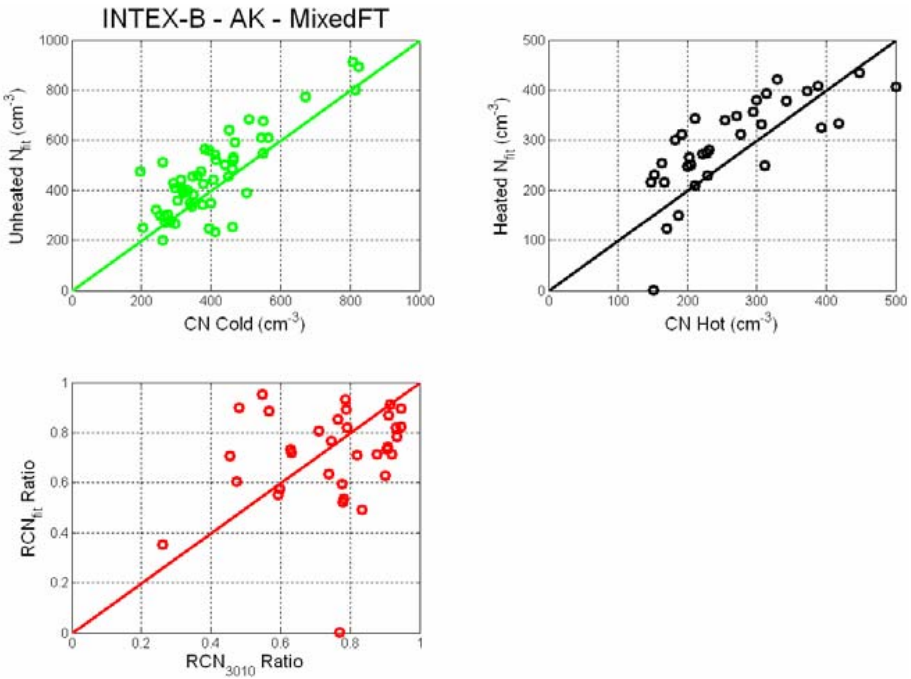

Fig. 4. Same as Fig. 2 but for data collected in the FT near Alaska.

ACPD
9, 8469–8539, 2009

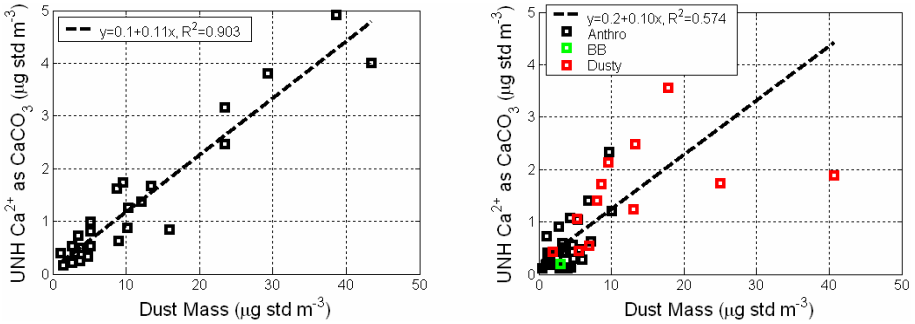

Fig. 5. Regressions of UNH Ca^{2+} as $CaCO_3$ versus size distribution integral mass (assumes density of 2.06 g cm^{-3}) for Hawaii (left) and Alaska (right). Regressions indicate an 11 wt% estimate for the mineral dust calcite content.

ACPD
9, 8469–8539, 2009

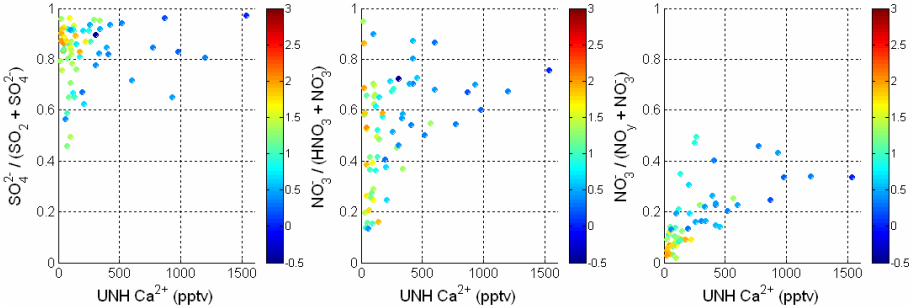

Fig. 6. Ratio of aerosol sulfur to total sulfur (left), aerosol nitrate to nitrate plus nitric acid gas (center) and aerosol nitrate to the sum of nitrogen species (right). Data are color coded by scattering Ångstrom exponents; large values (red) indicate pollution dominated airmasses, while small or negative values (blue) indicate presence of dust.

ACPD
9, 8469–8539, 2009

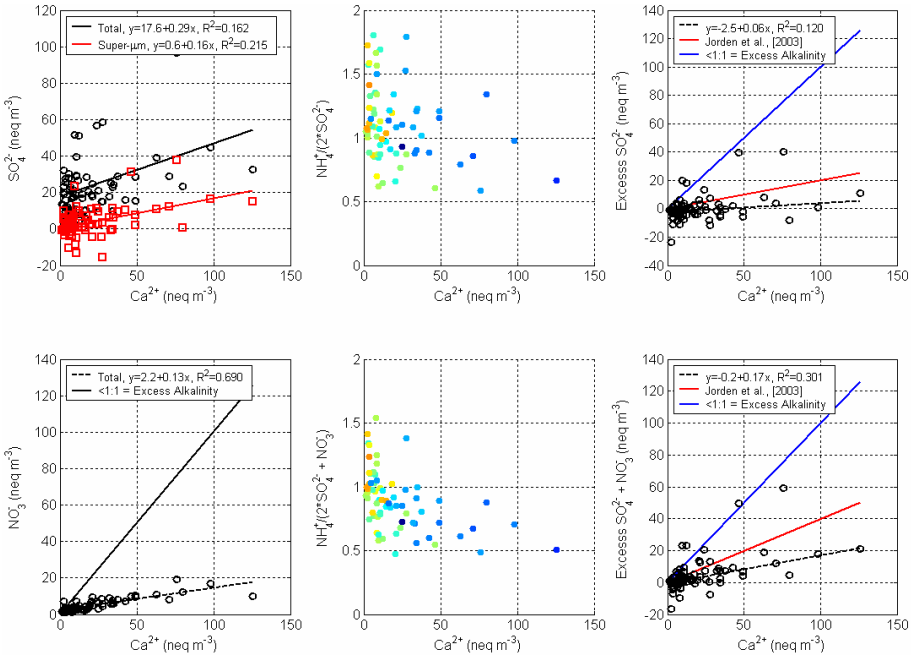

Fig. 7. Linear regression of sulfate and nitrate equivalents versus equivalents of calcium at SATP (left-column). Neutralization of sulfate and sulfate+nitrate by ammonium as a function of equivalents of calcium (middle-column) – data are color coded by scattering Ångstrom exponent as per Fig. 6. Excess sulfate and excess sulfate + nitrate plotted versus equivalents of calcium after the method of Jordan et al. (right-column).

ACPD
9, 8469–8539, 2009

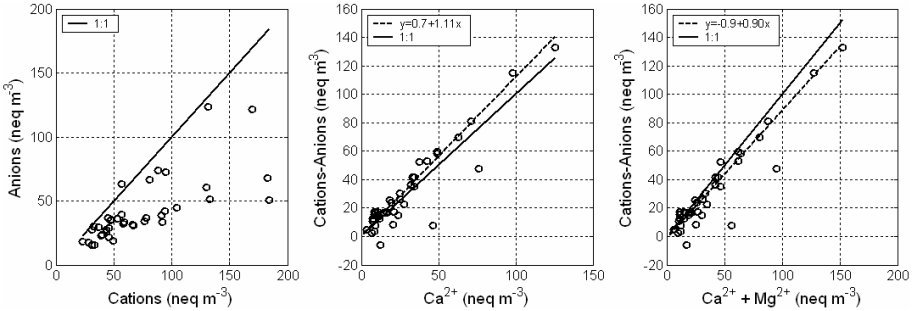

Fig. 8. Ratio of UNH anions to cations (left). Imbalances can be accounted for by assuming that the missing anion is CO_3^{2-} associated with calcite, $CaCO_3$ (center) or dolomite, $CaMg(CO_3)_2$ (right).

ACPD
9, 8469–8539, 2009

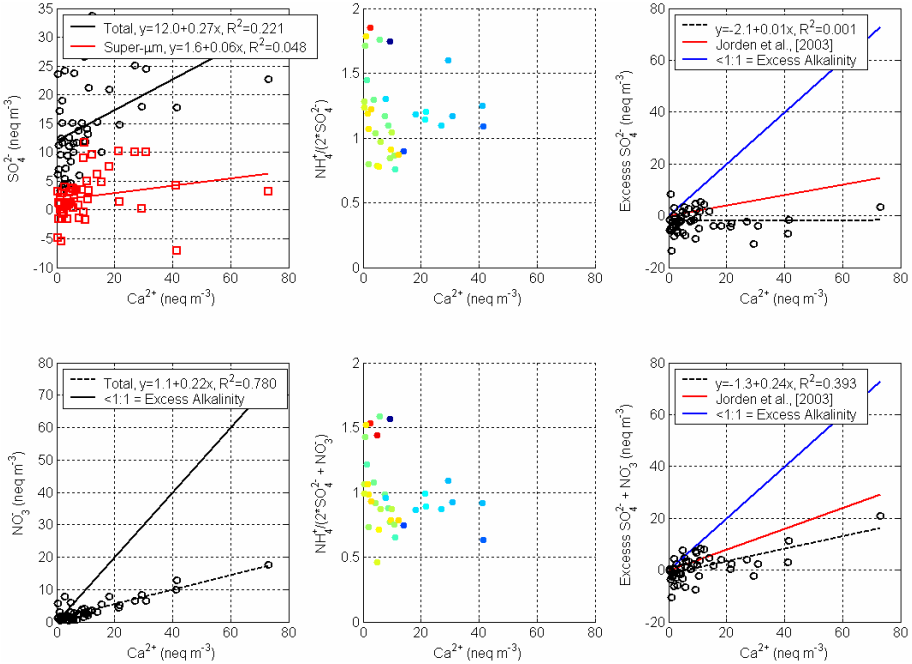

Fig. 9. Same as Fig. 7 but for tropospheric airmasses containing the stratospheric airmass tracer ^{7}Be. There is little correlation between supermicrometer sulfate and calcium but a relatively robust link between nitrate and calcium.

ACPD
9, 8469–8539, 2009

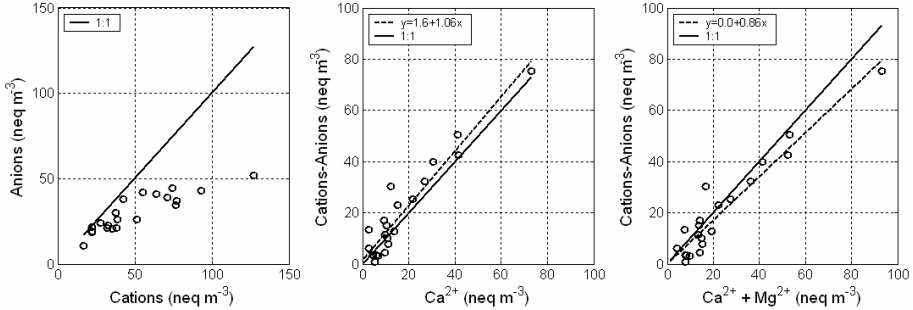

Fig. 10. Same as Fig. 8 but for tropospheric airmasses containing the stratospheric airmass tracer ^{7}Be. Anion-cation imbalance can be explained (±15%) by the presence of CO_3^{2-} as calcite or dolomite.

ACPD
9, 8469–8539, 2009

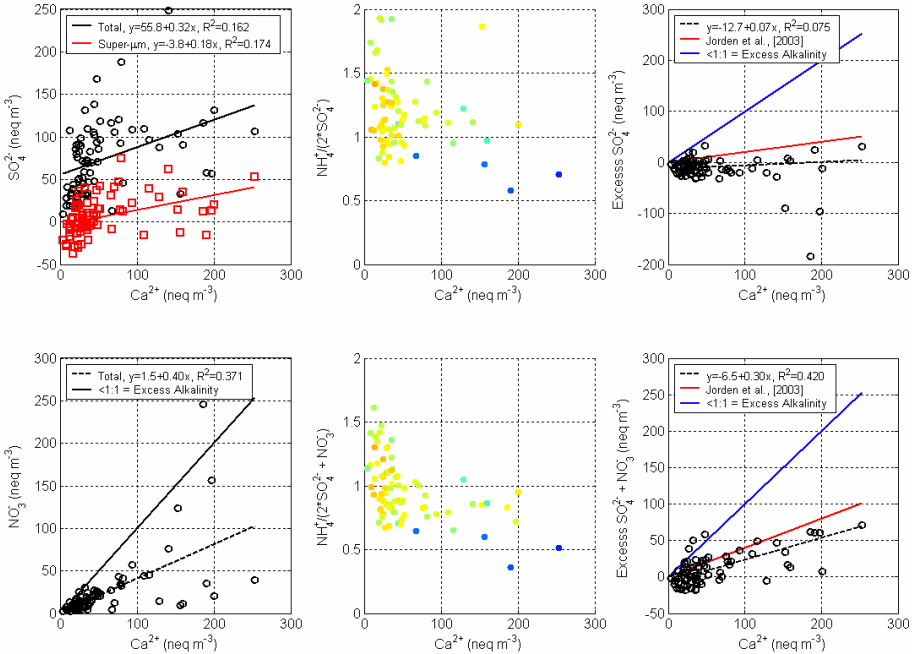

Fig. 11. Same as Fig. 7 but for airmasses in the continental boundary layer of the Central Mexican Plateau and the free troposphere above the Gulf of Mexico.

ACPD
9, 8469–8539, 2009

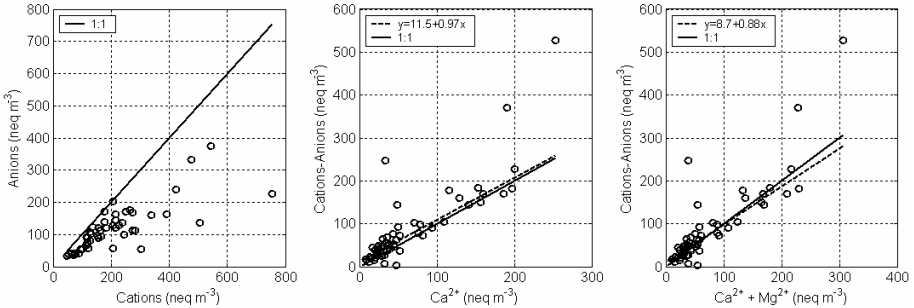

Fig. 12. Same as Fig. 8 but for airmasses in the continental boundary layer of the Central Mexican Plateau and the free troposphere above the Gulf of Mexico.

ACPD
9, 8469–8539, 2009

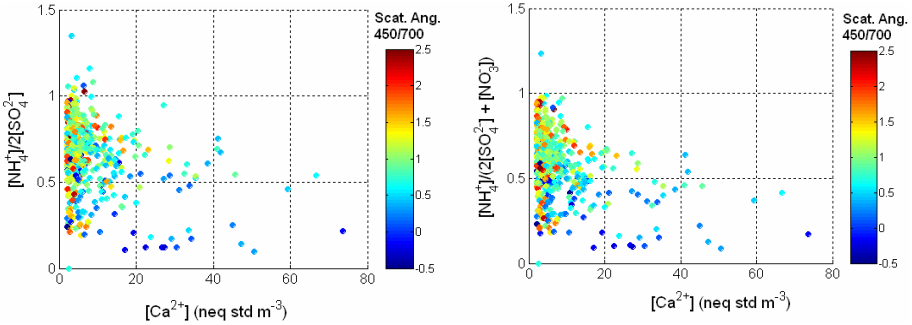

Fig. 13. Degree of sulfate neutralization by ammonium as a function of aerosol calcium (left). Degree of sulfate plus nitrate neutralization by ammonium as a function of aerosol calcium (right). Both plots are shaded by scattering Ångstrom exponent.

ACPD
9, 8469–8539, 2009

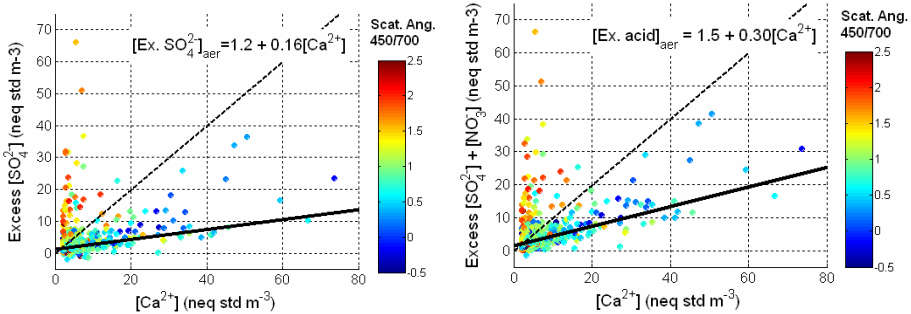

Fig. 14. Excess sulfate aerosol as a function of aerosol calcium (left). Excess sulfate plus nitrate as a function of aerosol calcium (right). Data below the dashed 1:1 line have not exhausted potential alkalinity if the Ca^{2+} is present as $CaCO_3$. Both plots are shaded by scattering Ångstrom exponent.

ACPD
9, 8469–8539, 2009

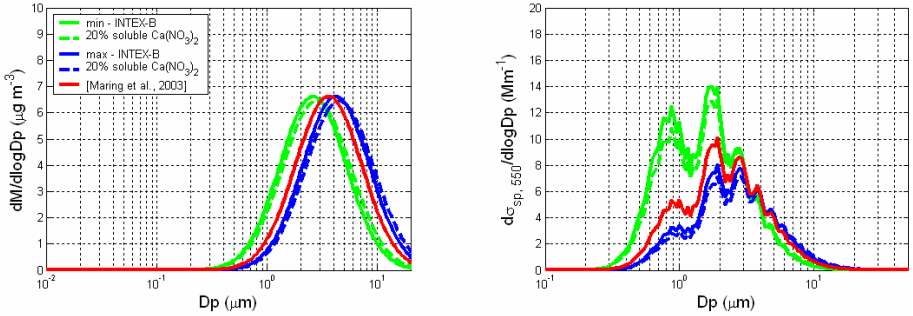

Fig. 15. Negligible increase in volume median diameter (left), and decrease in light scattering (right) as a result of heterogeneous conversion of 20 wt% of insoluble $CaCO_3$ to soluble $Ca(NO_3)_2$. Scattering is computed at 90% RH and uses a fixed refractive index of 1.53-0.0006*i*.

ACPD
9, 8469–8539, 2009

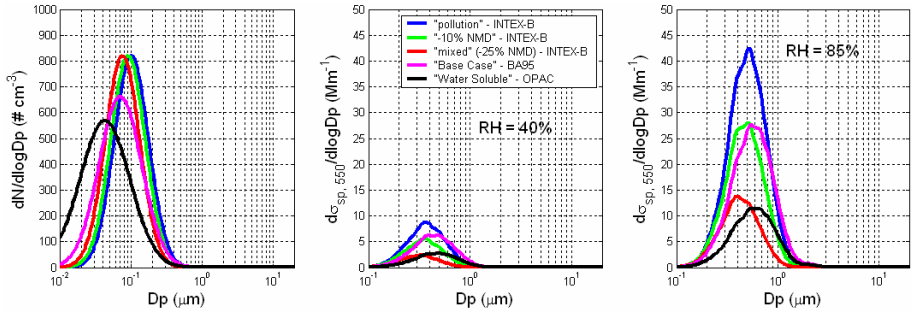

Fig. 16. Number size distributions (left) for INTEX-B data collected in pollution dominated cases (blue), mixed dust and pollution (red) for which there was a 25% reduction in the NMD. A 10% reduction in NMD is simulated in green while the base case of Boucher and Anderson (1995) is in magenta and the "water soluble" OPAC aerosol (Hess et al., 1998) is in black. Scattering size distributions at 40% RH (middle) and 80% RH illustrate the significance of NMD and σ_g on aerosol optical properties in the accumulation mode.

ACPD
9, 8469–8539, 2009

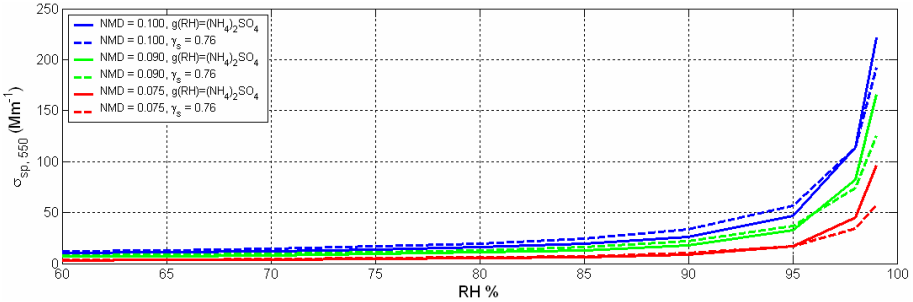

Fig. 17. Comparison of scattering as a function of RH calculated using Mie theory and assuming an $(NH_4)_2SO_4$ composition and an RH dependent refractive index (solid lines) for the three distribution in Fig. 16 compared to those using an estimated γ of 0.76 (dashed lines).

ACPD
9, 8469–8539, 2009

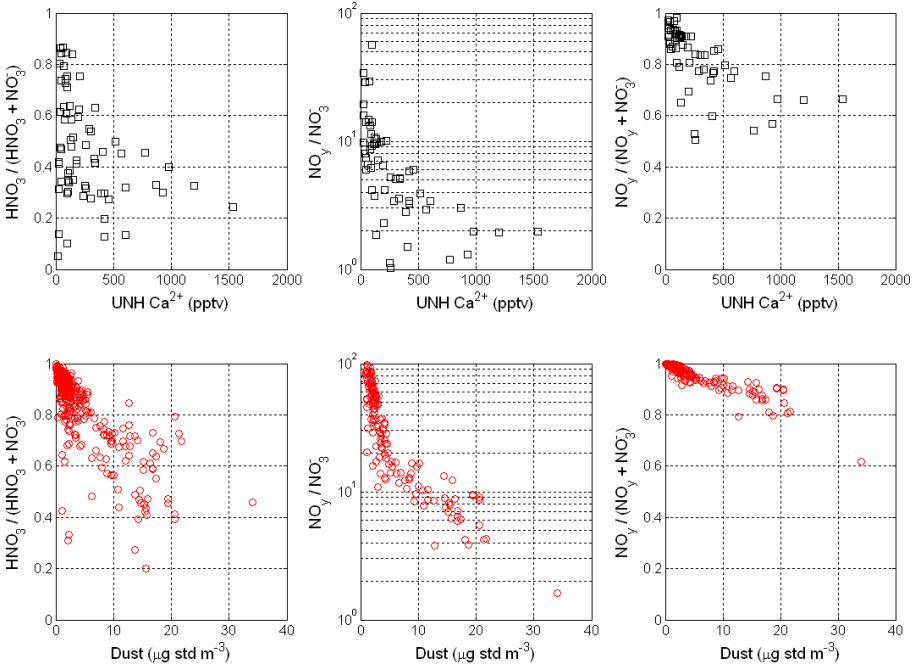

Fig. 18. Upper panels plot nitrogen ratios versus 300–600 s filter-based chemistry measurements of Ca^{2+}. Using an 11 wt% $CaCO_3$ and assuming 25% of the $CaCO_3$ has reacted to form $Ca(NO_3)_2$, the bottom panels attempt to replicate these relations using fast (60-s avg.) measurements of supermicrometer volume, i.e. mineral "dust" (ρ=2.06 g cm^{-3}).

ACPD
9, 8469–8539, 2009

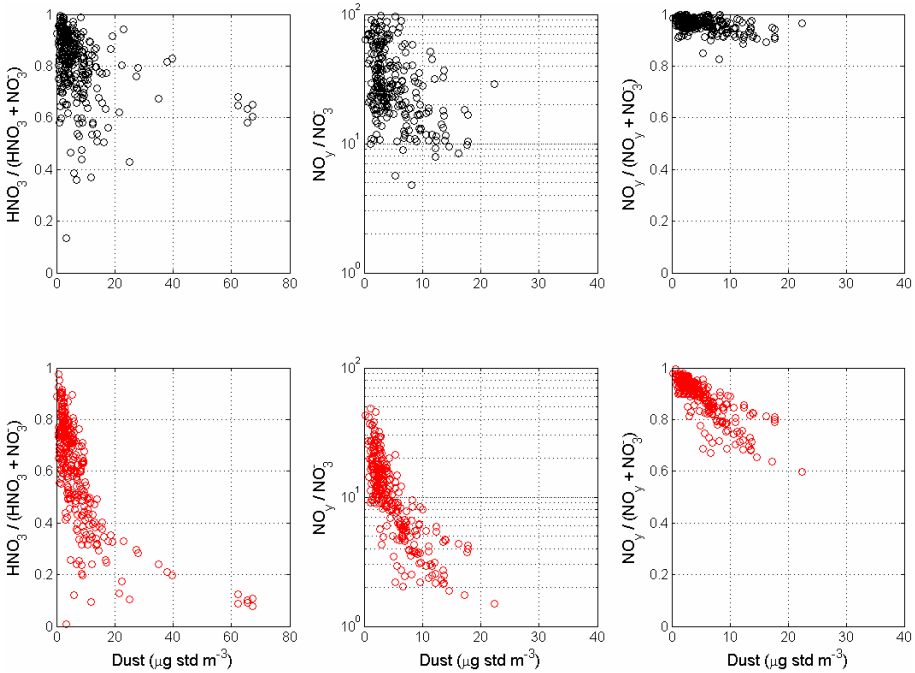

Fig. 19. Upper panels plot 60 s averages of gas phase and submicrometer aerosol nitrogen ratios versus fast (60-s avg.) measurements of supermicrometer volume, i.e. mineral "dust" (ρ=2.06 g cm^{-3}). Using an 11 wt% $CaCO_3$ and assuming 25% of the $CaCO_3$ has reacted to form $Ca(NO_3)_2$, the bottom panels attempt to replicate the NASA DC-8 measurements (top row – Fig. 18).

ACPD
9, 8469–8539, 2009